Original article

MOLECULAR METABOLISM

Ventromedial hypothalamic nucleus subset stimulates tissue thermogenesis via preoptic area outputs*

Rashmita Basu[1,2], Andrew J. Elmendorf[1,2], Betty Lorentz[2], Connor A. Mahler[2], Olivia Lazzaro[2], Britany App[2], Shudi Zhou[3], Yura Yamamoto[2], Mya Suber[2], Jamie C. Wann[4], Hyun Cheol Roh[4], Patrick L. Sheets[3], Travis S. Johnson[2,5,6], Jonathan N. Flak[1,2,*]

ABSTRACT

Objective: Hypothalamic signals potently stimulate energy expenditure by engaging peripheral mechanisms to restore energy homeostasis. Previous studies have identified several critical hypothalamic sites (e.g. preoptic area (POA) and ventromedial hypothalamic nucleus (VMN)) that could be part of an interconnected neurocircuit that controls tissue thermogenesis and essential for body weight control. However, the key neurocircuit that can stimulate energy expenditure has not yet been established.

Methods: Here, we investigated the downstream mechanisms by which VMN neurons stimulate adipose tissue thermogenesis. We manipulated subsets of VMN neurons acutely as well as chronically and studied its effect on tissue thermogenesis and body weight control, using *Sf1*^{Cre} and *Adcyap1*^{Cre} mice and measured physiological parameters under both high-fat diet and standard chow diet conditions. To determine the node efferent to these VMN neurons, that is involved in modulating energy expenditure, we employed electrophysiology and optogenetics experiments combined with measurements using tissue-implantable temperature microchips.

Results: Activation of the VMN neurons that express the steroidogenic factor 1 (Sf1; VMN^{Sf1} neurons) reduced body weight, adiposity and increased energy expenditure in diet-induced obese mice. This function is likely mediated, at least in part, by the release of the pituitary adenylate cyclase-activating polypeptide (PACAP; encoded by the *Adcyap1* gene) by the VMN neurons, since we previously demonstrated that PACAP, at the VMN, plays a key role in energy expenditure control. Thus, we then shifted focus to the subpopulation of VMN^{Sf1} neurons that contain the neuropeptide PACAP (VMN^{PACAP} neurons). Since the VMN neurons do not directly project to the peripheral tissues, we traced the location of the VMN^{PACAP} neurons' efferents. We identified that VMN^{PACAP} neurons project to and activate neurons in the caudal regions of the POA whereby these projections stimulate tissue thermogenesis in brown and beige adipose tissue. We demonstrated that selective activation of caudal POA projections from VMN^{PACAP} neurons induces tissue thermogenesis, most potently in negative energy balance and activating these projections lead to some similar, but mostly unique, patterns of gene expression in brown and beige tissue. Finally, we demonstrated that the activation of the VMN^{PACAP} neurons' efferents that lie at the caudal POA are necessary for inducing tissue thermogenesis in brown and beige adipose tissue.

Conclusions: These data indicate that VMN^{PACAP} connections with the caudal POA neurons impact adipose tissue function and are important for induction of tissue thermogenesis. Our data suggests that the VMN^{PACAP} → caudal POA neurocircuit and its components are critical for controlling energy balance by activating energy expenditure and body weight control.

Keywords Energy expenditure; Ventromedial hypothalamic nucleus; Thermogenesis; Preoptic area; Obesity; Pituitary adenylate cyclase activating peptide

1. INTRODUCTION

Upon a change in energy status, neural circuits dynamically balance caloric intake with energy expenditure to maintain body weight; obesity arises when these responses are no longer adequate. Our lack of understanding of the components and mechanisms that promote energy expenditure, are a barrier for obesity-treatment.

Basal metabolic rate (BMR) accounts for about 70% of total energy expenditure, followed by activity-induced thermogenesis from exercise and non-exercise activities (10–15% of total energy expenditure) and

*Reprint requests should be addressed to Jonathan N. Flak, PhD.

[1]Department of Pharmacology and Toxicology, Indiana University School of Medicine, Indianapolis, IN, USA [2]Lilly Diabetes Research Center, Indiana Biosciences Research Institute, Indianapolis, IN, USA [3]Department of Medical Neuroscience, Indiana University School of Medicine, Indianapolis, IN, USA [4]Department of Biochemistry and Molecular Biology, Indiana University School of Medicine, Indianapolis, IN, USA [5]Department of Biostatistics and Health Data Science, Indiana University School of Medicine, Indianapolis, IN, USA [6]Melvin and Bren Simon Comprehensive Cancer Centre, Indiana University School of Medicine, Indianapolis, IN, USA

*Corresponding author. Indiana Biosciences Research Institute 1210 Waterway Blvd., Ste. 2000, Indianapolis, IN 46022, USA. Tel.: +317 983 3315; fax: +317 983 3350. E-mail: jflak@indianabiosciences.org (J.N. Flak).

Received December 29, 2023 • Revision received April 20, 2024 • Accepted April 27, 2024 • Available online 8 May 2024

https://doi.org/10.1016/j.molmet.2024.101951

adaptive thermogenesis from ingesting food or being exposed to cold temperatures (10–15% of total energy expenditure) [1]. Unlike BMR, which is largely shaped by genetics, the other two are regulated by environmental stimuli such as temperature, hormone levels, and nutritional status. The brain integrates these environmental cues via bi-directional communication between the central nervous system (CNS) and the peripheral nervous system (PNS) that together regulate energy expenditure [2–5]. The sympathetic nervous system, stimulated by the CNS, induces adaptive thermogenesis in brown adipose tissue (BAT) and beige adipose tissue [6,7] to stimulate metabolic rate and promote weight loss via the action of norepinephrine [5,6,8]. CNS signals stimulates norepinephrine release from neurons in the sympathetic chain in response to exercise, cold temperature, and diet related signals, which then induces mitochondrial uncoupling protein 1 (UCP1) expression and lipolysis in brown and beige adipocytes. This triggers fatty acid oxidation and mitochondrial uncoupling, accompanied by heat production or thermogenesis as a by-product [9,10] which is an adaptive and plastic way to metabolize and remove excess nutrients from the system.

The ventromedial hypothalamic nucleus (VMN), a region within the medio-basal hypothalamus of brain, traditionally known for mediating glucose homeostasis, induces BAT thermogenesis, and downstream communication initiated by VMN neurons is crucial for energy expenditure control [11,12]. Our lab has shown that lesioning of the VMN leads to increased body weight and adipose mass along with a decrease in lean mass in mice compared to their littermate controls [13]. A subpopulation of VMN neurons densely expresses a neuropeptide called pituitary adenylate cyclase activating polypeptide (PACAP), encoded by *Adcyap1*. PACAP administration induces sympathetic nervous system activity, panic behavior, anorexia, and thermogenesis [14,15]. In addition, we previously demonstrated that loss of PACAP at the VMN, induces obesity without inducing hyperphagia and that VMN^{PACAP} neurons control energy balance by promoting energy expenditure [16]. Suppression of this neuropeptide within only the VMN occurs naturally in response to both fasting and decrease in leptin levels [17], which could be a critical signal to match energy expenditure with food intake.

Recent evidence indicates that distinct VMN neuron subsets project to different areas of the brain and mediate separate physiological effects via distinct neural circuits [18–20]. However, the neural circuit and the node downstream of VMN, that is involved in energy expenditure and body weight control remains undefined. Here, we aim to dissect the components and nodes of this neural circuit. Even though the VMN^{PACAP} neurons are a major regulator of energy expenditure and body weight, the mechanistic details are still unclear. Dissecting the physiological, cellular, and molecular bases of this neural circuit is key to understanding the central control of energy balance and its dysfunction during obesity. By doing this, we will expand our knowledge of the key neural systems that govern body weight independent from food intake.

2. MATERIALS AND METHODS

2.1. Animals

The procedures included in this manuscript were approved by the Committee on the Use and Care of Animals at Indiana University (Indianapolis, IN). All mice were provided with standard chow diet and water *ad libitum,* unless noted otherwise, and kept in a temperature-controlled (23 °C) room on a 12-hour light–dark cycle. $Sf1^{Cre}$ mice were generated by Bradford Lowell (Beth Israel deaconess Med Centre (Harvard)) (RRID:IMSR_JAX:037533) [21], *Adcyap1-2A-Cre* ($Adcyap1^{Cre}$) mice were generated by Zachary Knight (University of California, San Francisco (UCSF)) (RRID:IMSR_JAX:030155) [22]. All experiments were carried out using approximately equal numbers of male and female mice, unless noted otherwise. For HFD studies only male mice were used, since prevalent data shows female mice are resistant to diet-induced obesity. These mice were provided with high fat diet regimen (HFD; 45% kcal from fat, high sugar, D12451, Research Diets), starting from 8 to 10 weeks of age, till 40–44 weeks of age until they were at least 35 g body weight. Mice that weighed less than 35 g after 44 weeks age were removed from the study. Mice were group-housed prior to stereotaxic surgery in all cohorts, but single-housed post-operatively for body weight and food intake studies, indirect calorimetry, optogenetics and temperature measurements at adipose tissue depots. Otherwise, animals continued to be housed with their littermates. Unless stated, male and female mice were included for the analysis. All cre-driver mice were used in the homozygous state. All transgenic mice were maintained on a mixed background and have been described previously [13,16,23,24]. All mice were genotyped via polymerase chain reaction (PCR) across the genomic region of interest prior to study and only mice heterozygous for $Sf1^{Cre}$ or homozygous for $Adcyap1^{Cre}$ were included in the study. All mice were bred via in-house colonies. For studies, animals were processed in the order of their ear tag number, which was randomly assigned at the time of tailing (prior to genotyping). Investigators were blinded to genotype/treatment for all studies except knock-out experiments.

2.2. Reagents

All the AAVs were acquired from Addgene (Addgene HQ Addgene, Watertown, Massachusetts). All AAVs were aliquoted into 3ul stocks upon arrival and stored at −80C. AAV-hSyn-DIO-hM3Dq-mCherry (2.1×10^{13} GC/ml), Addgene plasmid 44361, serotype 8; AAV-hSyn-DIO-mCherry (2.2×10^{13} GC/ml), Addgene plasmid 50459, serotype 8; AAV-hSyn-FLEx-mGFP-2A-Synaptophysin-mRuby (7×10^{12} GC/ml), Addgene plasmid 71760, serotype 1; AAV-Ef1a-DIO-hChR2-eYFP (2.2×10^{13} GC/ml), Addgene plasmid 35507, serotype 9; AAV-Ef1a-DIO -eYFP (2.2×10^{13} GC/ml), Addgene plasmid 35507, serotype 9; AAV-hSyn-hM4Di-mCherry (2×10^{13} GC/ml), Addgene plasmid 50475, serotype 8, [gifted by Bryan Roth, UNC to Addgene].

2.3. Stereotaxic injections of viral constructs

Craniotomy was performed on $Sf1^{Cre}$ mice aged 18-20 week-old mice that weighed at least 35 g $Adcyap1^{Cre}$ mice received a craniotomy at ages 8–14 weeks old. All mice were anesthetized with 1.5–2% isoflurane, in preparation for craniotomy. Successful anesthesia of the mice was tested by hind-leg pinch. The animal was placed on a warm water heating pad, kept at 37 °C, on the stereotaxic platform (Kopf) and its head was fixed using the ear-bars and nose piece. The eyes were covered with Artificial Tears ointment (Pivetal) to avoid drying of the eyes. The scalp was shaved, and the shaved area was disinfected with 10% iodine solution (PVP) (Medline) followed by sterile PBS. After exposing the skull with an incision, bregma and lambda were leveled, a hole was drilled, and the contents of a pulled pipette at the coordinates of our target were released at ∼10 nl/min. For the VMN-directed injections in $Sf1^{Cre}$ mice, 150 nl of virus were injected at anteroposterior (AP) −1.05, mediolateral (ML) +/− 0.35, dorsoventral (DV) −5.55. For the tracer studies 75 nl of virus was injected at the VMN of $Adcyap1^{Cre}$ mice at AP -1.05, ML +/− 0.35, DV -5.55. For optogenetic studies using $Adcyap1^{Cre}$ mice, 75 nl of virus was injected unilaterally at the VMN, at AP -1.05, ML - 0.35, DV -5.55, followed by

mono fiber-optic cannula (Doric lenses, size 5.8 mm) implantation at a 45° angle at the VMN unilaterally at AP -1.05, ML - 2.05, DV -5.4. Additionally, another mono fiber-optic cannula (Doric lenses, size 5.8 mm for caudal POA or 4.5 mm for the bed nucleus of stria terminalis (BNST) was implanted unilaterally at either of the two VMN outputs: (1) for caudal POA at AP +0.1, ML - 0.56, DV -5.3; (2) BNST at AP +0.6, ML - 0.65, DV -4.3. The mono fiber-optic cannulas were fixed with 2 mixtures: (i) and (ii). Mixture (i) contained C&B METABOND and AMALGAMBOND: 5 mg AMALGAMBOND, 4 drops of B METABOND and 1 drop of C Universal catalyst. This was allowed to solidify for 3 min and was followed by mixture (ii), a dental cement (mixture of Contemporary Ortho-Jet Powder and Contemporary Ortho-Jet liquid, Lang Dental Manufacturing Co., Inc.) on top of the skull. For optogenetic activation at VMN combined with inhibition at caudal POA studies using *Adcyap1*^{Cre} mice, 75 nl of AAV-Ef1a-DIO-hChR2-eYFP virus (for cre-dependent expression) was injected at the VMN, at AP -1.05, ML - 0.35, DV -5.55, and AAV-hSyn-hM4Di-mCherry virus (for cre-independent local neuronal expression) was injected at the caudal POA, at AP +0.1, ML - 0.56, DV -5.54 followed by a mono fiber-optic cannula (Doric lenses, size 5.8 mm) implantation unilaterally at caudal POA at AP +0.1, ML - 0.56, DV -5.3. For all surgeries, we allowed at least 5 min for the virus to diffuse into the brain and the pipette was raised slowly out of the hole in the skull. The hole in the skull where the virus was injected was filled with bone wax. The skin incision was closed with surgical glue (VetBond, 3M). Analgesics (Carprofen, 5 mg/kg) were administered prophylactically to all mice to prevent post-surgical pain. The mice were allowed four weeks to recover from surgery before any experimental manipulation. Either mCherry or YFP fluorescent reporters were used to confirm proper targeting of the brain region in all studies. If fluorescence was not observed within the VMN, these cases were omitted from analyses.

2.4. Phenotypic studies

Body weight and food intake were monitored weekly in all mice post-surgery. Body weight and food were weighed weekly on a precision balance (OHAUS Corporation, model # SPX421). Glycemic measures were performed on the *Adcyap1*^{Cre} mice for optogenetic studies. Blood glucose was measured with a One Touch Ultra 2 glucometer (Johnson and Johnson) by tail vein draw. For all glycemic measures, mice were fasted for 5 h prior to testing. Additionally for the glycemic measures in fasted state, mice were fasted for 24 h before measuring blood glucose. Body composition data was collected with assistance from Indiana University School of Medicine Mouse Metabolic Phenotyping Center from the EchoMRI™-100H Body Composition Analyzer. TSE Phenomaster cages were used for indirect calorimetry measurement, with assistance from the Indiana University School of Medicine Mouse Metabolic Phenotyping Center. Indirect calorimetry data was used to calculate fat oxidation and glucose oxidation via the Weir equation.

2.5. Temperature at adipose tissue depots

During stereotaxic surgeries, temperature programmable microchips (UCT-2112 Temperature Microchip), from UID (Lake Villa, Illinois), were implanted using UPGI-Q Pistol Grip Injector from UID, directly underneath the skin, above the interscapular brown adipose tissue (iBAT) and inguinal white adipose tissue (or beige adipose tissue; iWAT) in *Adcyap1*^{Cre} mice. Animals were allowed 4-week recovery and acclimation was performed by handling them and using the handheld reader system (UID, model URH-1HP) or the automated system (UID, home cage monitoring system) for 5 consecutive days before taking the final measurements. Data were collected using the handheld reader system at the time points indicated or continuously using the automated system.

2.6. Acute brain slice preparation

After the recovery from intracranial injections, acute brain slices were prepared as described previously. Mice were briefly (∼15 s) anesthetized with 99.9% isoflurane (Patterson Veterinary) and quickly decapitated. Brains were rapidly dissected and submerged in an ice-cold choline solution containing the following (in mM): 110 choline chloride, 25 $NaHCO_3$, 25 D-glucose, 11.6 sodium ascorbate, 7 $MgSO_4$, 3.1 sodium pyruvate, 2.5 KCL, 1.25 NaH_2PO_4, and 0.5 $CaCl_2$). Coronal brain slices containing the pre-optic region (spine of the blade tilted rostrally 15° off vertical plane, 300-μm thick) were prepared with a vibratome (VT1200S; Leica). Slices were transferred to a 37 °C artificial CSF (ACSF) bath containing the following (in mM): 127 NaCl, 25 $NaHCO_3$, 25 D-glucose, 2.5 KCl, 1$MgCl_2$, 2 $CaCl_2$, and NaH_2PO_4 for 30 min. Slices were subsequently incubated for at least 45 min in ACSF at room temperature before being transferred to the recording chamber.

2.7. Electrophysiological recordings

Slices were placed in the recording chamber of a SliceScope Pro 6000 (Scientifica) and continuously perfused with the ACSF (30–32 °C) at the rate of ∼1 ml per minute. Slices were held in place with a slice anchor (Warner Instruments). Recording pipettes were made from borosilicate capillaries with filaments (G150-F; Warner Instruments) using a horizontal pipet puller (P-97; Sutter Instruments). Pre-optic neurons approximately 40 μm or deeper from the surface of the slice were targeted for recording. After establishing a Gigaohm (GΩ) seal between the pipette tip and the cell membrane gentle negative pressure was applied from inside the pipette to open the cell membrane. After the opening of the cell membrane, neurons were allowed to stabilize for 5 min before recording. The patch electrode (2.5–3.5 MΩ resistance) was filled with a cesium-based internal was used: 60 mM CsMeSO3, 60 mM CsCl2, 10 mM HEPES, 0.2 mM EGTA, 8 mM NaCl, 2 mM MgCl2, 3 mM MgATP, 0.3 mM NaGTP, 5 mM lidocaine, 10 mM phosphocreatine. Whole-cell patch-clamp recordings were performed at 30–32 °C, amplified and filtered at 4 kHz, and digitized at 10 kHz using a Multiclamp 700B amplifier (Molecular Devices). Evoked excitatory postsynaptic currents and evoked inhibitory postsynaptic currents (eEPSCs/eIPSCs) were generated by initiating blue lights using a LED illumination system (CoolLED pE-4000) using a 490 nm wavelength LED with a GFP filter (ET FITC/GFP, Olympus). Membrane potential was held at −60 mV in a voltage-clamp mode for eEPSCs and at +10 mV for eIPSCs. No synaptic blockers were added during evoked electrophysiological recordings. After the recording, CPP and NBQX (Tocris, Bristol, UK; 5 μM) were added to the ACSF to block glutamatergic (excitatory) inputs; SR 95531 hydrobromide (GABAzine, Tocris, Bristol, UK; 10 μM) was added to the ACSF to block GABAergic (inhibitory) inputs. Pipette capacitance was compensated, and the inclusion of data required a series resistance <35 MΩ.

2.8. Optogenetics

For the optogenetic measurements, the optical fibers in the head of the singly housed *Adcyap1*^{Cre} mice were connected to a blue light (450 nm) emitting optical system (Doric Lenses, LED Illumination system), using fiber optic patch cords, that were attached to fiber optic cannulas on the skull, and stimulated at VMN along with either of the two VMN efferents (either caudal POA or BNST). Blue light stimulation was done using 120 mA current at 40Hz frequency for 5.0 ms.

Glycemic measures and measurements for temperature at the different adipose tissue depots were done-first without blue light stimulation for 90 min and then with lights on for 120 min. For the studies with optogenetic activation at VMN combined with hM4Di mediated inhibition at caudal POA, the *Adcyap1*^{Cre} mice were injected with clozapine-N-oxide (CNO) (0.3 mg/kg, IP) 30 min prior to blue light stimulation. For these mice the optogenetic stimulation was done following CNO injection, as mentioned above. All mice in the optogenetics studies were acclimated for at least a week to the laser equipment and procedure room prior to testing to ensure a low stress environment. Mice were tested within their home-cages and were allowed to freely move around their home-cage.

2.9. Terminal tissue collection

After completion of phenotypic and/or physiological studies, the mice were terminally sacrificed for tissue harvesting. For studies with hM3dq, the mice were injected with CNO (0.3 mg/kg, IP) 2 h prior to tissue collection. For optogenetic studies, mice were either stimulated with blue light or no blue light for the respective control group for 2 h prior to tissue collection. At the end of the 2 h of treatment, mice were anesthetized with isoflurane for harvesting. All mice were anesthetized with isoflurane. When deeply anesthetized, adipose tissues: iBAT, iWAT and perigonadal white adipose tissue (pgWAT) were collected immediately prior to transcardial perfusion and immediately placed on dry ice.

2.10. Perfusion and immunohistochemistry

Brains from mice were collected and processed as previously described [13,16,23,24]. Following terminal tissue harvest, transcardial perfusion was performed on the mice with phosphate buffered saline (PBS) followed by 10% neutral buffered formalin (NBF) (Fisher brand, catalog #245685). Brains were removed and placed into 10% NBF overnight, followed by 30% sucrose for at least 36 h. Brains were cut into 30 μm sections on a freezing microtome in four series and stored in antifreeze solution (25% ethylene glycol, 25% glycerol). For immunohistochemistry staining sections were washed with PBS and then treated sequentially with 1% hydrogen peroxide/0.3% sodium hydroxide, 0.3% glycine, and 0.03% sodium dodecyl sulfate. Pretreatment was followed by an hour in blocking solution (PBS containing 2.5% triton, 3% Normal Donkey Serum [Lampire Biological Laboratories, catalog # 7332100]), followed by overnight incubation in blocking solution containing either chicken anti-GFP (GFP-1020, RRID: AB_1000240, Aves, 1:1000) or rabbit Living Colors DsRed Polyclonal Antibody (632496, RRID: AB_10013483, Takara Bio 1:1000). The next day, the sections were incubated with fluorescent secondary antibodies: either Cy™3 AffiniPure Donkey Anti-Rabbit IgG (H + L) (711165152, RRID: AB_2307443, Jackson) with DsRed or Alexa Fluor® 488 AffiniPure Donkey Anti-Chicken IgY (IgG) (H + L) (703-545-155, RRID: AB_2340375, Jackson) with anti-GFP. cFos staining was done additionally to the slices to quantify neuronal activation. For this cFos staining was done in day 1 of staining using Rabbit anti-c-Fos antibody (2250S c-Fos 9F6, RRID: AB_, Cell Signaling) followed by Peroxidase AffiniPure Donkey Anti-Rabbit IgG (H + L) (711-035-152, RRID: AB_10015282, Jackson). This was followed by the DsRed or GFP staining as described above. The stained sections were mounted onto slides and cover slipped with Fluoromount-G (Southern Biotech).

2.11. Total RNA-sequencing

100 mg of iBAT and iWAT were each homogenized using Bullet Blender. Steel beads were used to homogenize iBAT and zirconium oxide beads were used to homogenize iWAT. RNA was extracted from the homogenized tissue using the TRIzol® Reagent (15596018, Ambion) and PureLink™ RNA Mini Kit with on-column DNase I (Zymo Research DNase I; catalog # E1010). The RNA quality and concentration was checked by Nanodrop 2000 (Thermo Scientific). Total RNA sequencing was done by the Centre for Medical Genomics Core at Indiana University School of Medicine. The RNA sequencing data was then analyzed by Olivia Lazaro under the supervision of Dr. Travis Johnson. Analysis was performed separately for each type of adipose tissue parallely using RStudio (version 4.1.1). The reads were aligned using the package Rsubread (version 1.22.2) and annotated using the GRCm38 primary assembly through the index building function in Rsubread [25–31]. The BAM files generated through paired end alignment were then mapped to obtain read counts. These counts were annotated based on experimental group and sex, then filtered for expression to remove genes with an average expression of less than 1 CPM across all samples. The filtered data was then used to create a design matrix using model.matrix () from the limma package (version 3.50.1) with explanatory variables based on sample sex and treatment group for both sexes combined, but adjacently the same pipeline was run for each individual sex for comparative analysis using only the explanatory variable of treatment group. This design matrix is used for the standard limma RNAseq pipeline [25–27] consisting firstly of the voom function, which estimates the mean-variance of the log-counts, then generates precision weights for each observation, which are used for linear model fitting for each gene. The generated linear model is then used to compute an array containing the logFC (log fold change) value, p value, adjusted p value (by Benjamini-Hochberg procedure), average expression, and log-odds of differential expression for each gene using the empirical Bayes method [28]. This array was filtered for all genes meeting the criteria of having an adjusted p value less than 0.05 and a logFC value greater than 0.58 or less than −0.58, which were considered to be differentially expressed. Volcano plots were generated using the ggplot2 package (version 3.3.6) to visualize the genes based on scaled (from −1.0 to 1.0) logFC values and scaled (from 0 to 1) adjusted p values, and heatmaps using the heatmap3 package (version 1.1.9) based on gene expression for each of the top 20 DEGs for each group. Finally, the expression values for all upregulated and downregulated DEGs are subset and used for functional enrichment using clusterProfiler (version 4.2.2) with annotation sourced from AnnotationDbi (version 1.56.2) [29–31] and visualization of results using enrichplot (version 1.14.2).

2.12. Quantitative real-time PCR

RNA was isolated in a similar fashion as described in section 2.11. cDNA was synthesized by reverse transcription from mRNA (extracted using the method described above) using the SuperScript VILO cDNA Synthesis Kit (Invitrogen). Gene expression was performed by quantitative real time PCR (qRT-PCR) using Taqman gene expression assays using TaqMan Fast Advanced Master Mix (Thermo Fisher) with a standard protocol using the applied biosystems' setup and Quantstudio 5 and Quantstudio 3 (Thermo Fisher Scientific). Gene expression was measured for *Ucp1* (Mm01244861_m1), *Dio2* (Mm00515664_m1), *Ppargc1a* (Mm01208835_m1), *Prdm16* (Mm00712556_m1), *Cidea* (Mm00432554_m1), *Elovl3* (Mm00468164_m1), *Zbtb16* (Mm01176868_m1), *MaeA* (Mm00491367_m1), *Slc26a8* (Mm00524836_m1), *Ppt1* (Mm00477078_m1), *Kdm6b* (Mm01332680_m1). Relative abundance for each transcript was calculated by a standard curve of cycle thresholds and normalized to TBP (Mm01277042_m1).

2.13. Cell counts

Images from 30 μm thick sections containing DsRed or GFP alone or with cFos antibody staining were collected in the VMN, POA, BNST, paraventricular thalamus (PVT) and periaqueductal gray (PAG) using an Echo Fluorescent microscope with a 4× or 10× objective. The target regions were identified by overlaying the corresponding bregma level from an anatomical reference using The Mouse Brain in Stereotaxic Coordinates Fourth Edition (Paxinos and Franklin) on microscope images. Images were collected with the same exposure settings on the microscope. They were counted by eye using the counting feature in ImageJ by someone blind to treatment. Total number of cFos-IR nuclei were counted for each brain area on one side.

2.14. Statistics

Time-course data for the following studies: body weight, food intake, blood glucose and temperature at adipose depots, were analyzed by two-way repeated measures ANOVA with Fisher's LSD post hoc test. Data in Figures 1C, 3C—K, 4B—J, 7B,E, S3A—S3F were analyzed by two-way repeated measures ANOVA with Fisher's LSD post hoc test. Data in Figures 1D—F, 1K, 2H, 7D, 7G, S2D, S2G, S2K, S20, S2R, S4A-S4B, S5C, S5F, S5I, S5J, S5M, S5P, S5Q were analyzed by student's t-test. Data in Figures 1G—L, 7C, F were analyzed by one-way ANOVA. Data was expressed as mean +/− SEM. No data were removed unless the injection missed the targeted location, or the animal was sick or injured at the time of the experiment (loss of >10% body weight). Significance was determined at $p \leq 0.05$. All data were analyzed using Prism (GraphPad, La Jolla, California).

3. RESULTS

3.1. Activating VMN^{Sf1} neurons blunts diet induced obesity in male mice

Previous studies from our lab showed that silencing the Sf1 neurons in the VMN (VMN^{Sf1}) led to obesity with a decrease in energy expenditure [13]. But their role in curbing diet induced obesity has not been identified. To test the potential for VMN^{Sf1} neurons to reduce body weight and adiposity in diet induced obesity, we put male *Sf1^{Cre}* mice on HFD. We first looked at pertinent phenotypic alterations. *Sf1^{Cre}* male mice and their littermate (WT) male controls were given HFD, beginning at 8—10 weeks of age, for 40—44 weeks of age until they weighed at least 35 g. We then performed craniotomy to administer *AAV$^{DIO\text{-}hM3dq\text{-}mCherry}$* (Figure 1A; Supplementary Fig. S1A) into the VMN of these mice (Supplementary Figs. S1B—S1C) and monitored their body weight, body composition, food intake and energy expenditure (Figure 1B). For the phenotypic measurements, *Sf1^{hM3dq}* mice and their WT littermate controls were acclimated for 7 days with once daily intraperitoneal (IP) saline injection. For the next 3 days they were injected with IP CNO, twice daily (every 12 h). Both groups of mice weighed the same before and 4-weeks post-surgery. After activating the *Sf1^{hM3dq}* neurons with IP CNO injection, *Sf1^{hM3dq}* mice lost 1g body weight in just 3 days, in contrast to the WT controls (Figure 1C), without altering food intake (Figure 1D). These mice also had 15% reduced adiposity (Figure 1E), and 5% increased lean mass (Figure 1F). To perform indirect calorimetry measurements, we included a separate cohort of these mice groups that were placed into the TSE metabolic

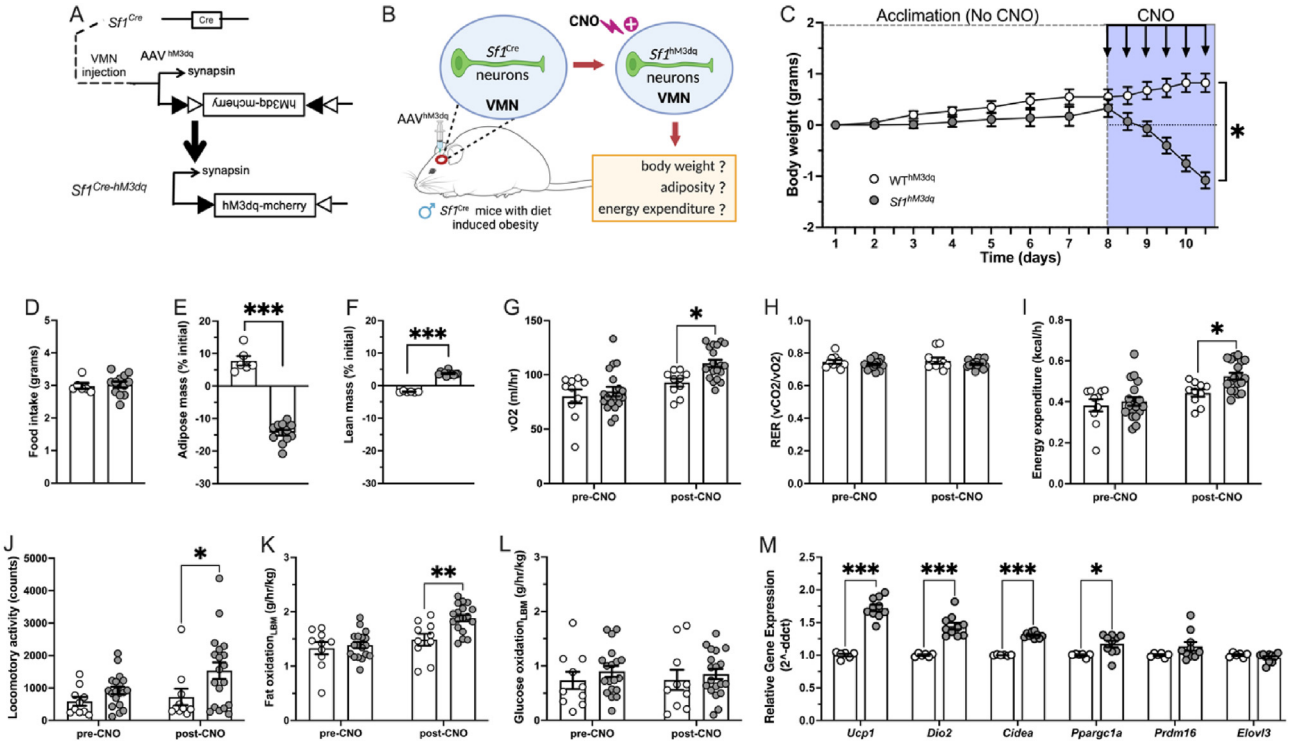

Figure 1: Activating VMN^{Sf1} neurons blunts diet induced obesity in male mice. We introduced *AAV$^{DIO\text{-}hM3dq\text{-}mCherry}$* into the VMN of either *Sf1^{Cre}* mice or their wild-type littermate controls (A). Then we tested the potential for activating VMN neurons in diet-induced following Clozapine-N-oxide (CNO) IP injection (B) and measured body weight (C) food intake (D), adiposity (E) and lean mass (F). Using TSE chambers, we also measured vO2 (G), RER (H), energy expenditure (I), locomotory activity (J), fat oxidation (K) and glucose oxidation (L) and compared the parameters between the *Sf1^{Cre}* mice and their wild-type littermate controls as well as between 3 h pre-CNO and 3 h post-CNO. qRT-PCR was done for thermogenic markers in iBAT (M), which was harvested post- 2 h IP CNO injection and before perfusion. n = 5—12 male mice. Data expressed as mean ± SEM and analyzed by either two-way RM ANOVA (C), by student's t test (D-F, K) or one-way ANOVA (G—J). *p < 0.05, **p < 0.01, ***p < 0.0001.

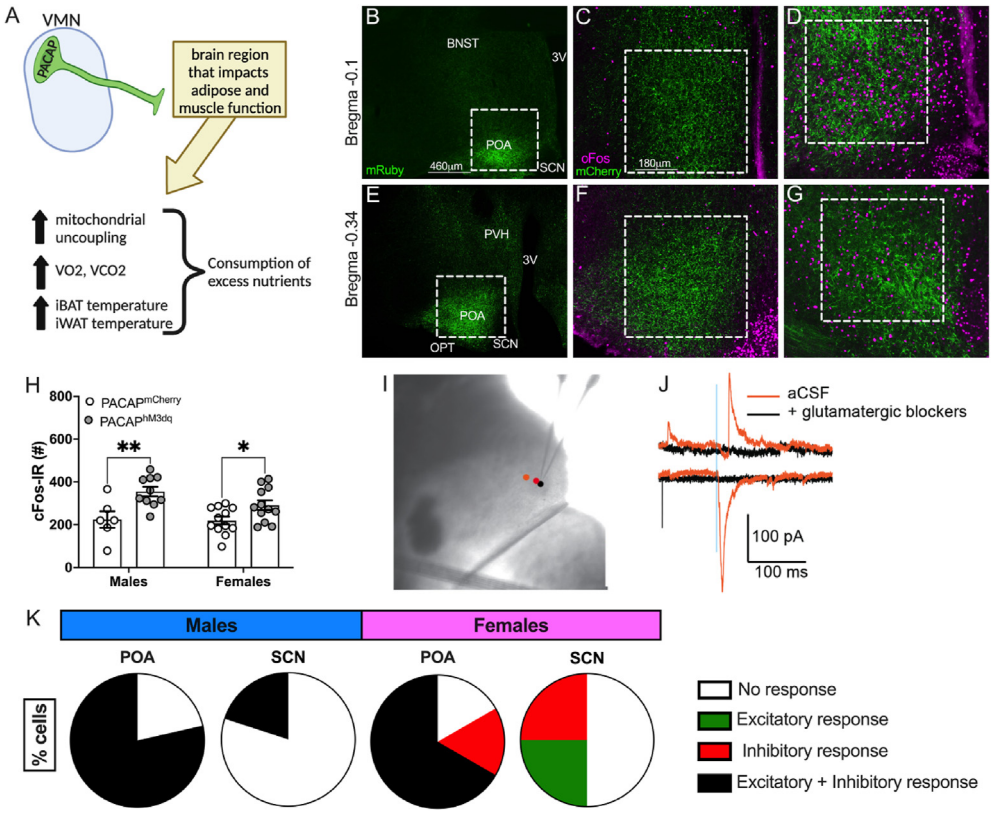

Figure 2: VMN^{PACAP} neurons send projections to the POA, thereby activating these neurons via glutamatergic signaling. We identified a new site that VMN^{PACAP} neurons project to, using *AAV$^{DIO\text{-}syn\text{-}mRuby}$* to see the projections from VMN and AAV$^{DIO\text{-}hM3dq}$ to measure neuronal activation via cFos induction. We observed projections (B,E) from VMN *Adcyap1^{Cre}* neurons and cFos following IP CNO (C-D, F-G) in the POA and counted (H). Scalebar = 180 μm. In addition, we recorded from 12 caudal POA neurons while activating ChR2-positive fibers from VMN *Adcyap1^{ChR2}* neurons in both normal CSF and in the presence of either glutamate (CPP and NMQX, 5 μM) blockers and the percentage of caudal POA neurons activated or inhibited are counted (I–K). Representative traces are included (I). (H) N = 6–10 mice. (J–K) N = 19 cells (14 POA, 5 SCN) from 3 male mice and N = 10 cells (6 POA, 4 SCN) from 3 female mice. 3V = 3rd ventricle. PVH = Paraventricular hypothalamic nucleus. SCN = Suprachiasmatic nucleus. OPT = Optic tract. Data expressed as mean ± SEM and analyzed by student's t test (H), *p < 0.05, **p < 0.01.

chambers. Then mice were acclimated for 4 days with once daily IP saline injection. The next 3 days they were injected with IP CNO, once daily. We compared the oxygen consumption (vO2), respiratory exchange rate (RER), energy expenditure, locomotor activity, fat oxidation and glucose oxidation between *Sf1^{hM3dq}* mice and the WT control groups, as well as the levels of those parameters at 3 h before IP CNO injection (pre-CNO) and 3 h after IP CNO injection (post-CNO). vO2 (Figure 1G) and energy expenditure (Figure 1I) were elevated, with no change in RER (Figure 1H), post-CNO injection in the *Sf1^{hM3dq}* mice. These mice also exhibited higher locomotory activity (Figure 1J) and elevated fat oxidation when normalized to their lean body mass (Figure 1K), with no change in the rate of glucose oxidation when normalized to their lean body mass (Figure 1L). We next measured expression of targets associated with thermogenesis (Figure 1M) in iBAT, using qRT-PCR, from iBAT harvested after 2-hour stimulation with IP CNO injection. Mitochondrial uncoupling protein 1 (*Ucp1*) (Figure 1M), iodothyronine deiodinase 2 (*Dio2*) (Figure 1M), cell death-inducing DNA fragmentation factor-like effector A (*Cidea*) (Figure 1K) and peroxisome proliferator-activated receptor gamma coactivator 1-alpha (*Ppargc1a*) (Figure 1M) were all upregulated in the *Sf1^{hM3dq}* mice compared to the controls. However, we did not observe any differences in the PR domain containing 16 (*Prdm16*) (Figure 1M) and elongation of very long chain fatty acids-3 (*Elovl3*) (Figure 1M). These data, taken together with the indirect calorimetry and phenotypic measurements, indicate that the mice with activated VMN^{Sf1} neurons have an elevated capacity for thermogenesis, which could contribute to their loss of body weight and adipose mass.

3.2. VMN^{PACAP} neurons send projections to the POA, thereby activating these neurons via glutamatergic signaling

We next investigated the efferent nodes of the VMN^{PACAP} neurons through which they transmit the signal downstream to the periphery (Figure 2A). To test where these neurons project to, we administered *AAV$^{DIO\text{-}syn\text{-}mRuby}$* at the VMN of 8–12 weeks-old *Adcyap1^{Cre}* mice to identify where the terminals are most concentrated in the brain (Figure 2B,E, S2A, S2H, S2L). In a separate cohort of mice, we administered *AAV$^{DIO\text{-}hM3dq\text{-}mCherry}$* or *AAV$^{DIO\text{-}mCherry}$* at the VMN of 8–12 weeks-old *Adcyap1^{Cre}* mice to identify which of the projection sites exhibit cFos after activating VMN^{PACAP} neurons. We activated the VMN^{PACAP} neurons using IP CNO injections and observed projections (Figure 2B, E) from the VMN^{PACAP} neurons and cFos following IP CNO (Figure 2C–D, F–G) in the POA using fluorescence and counted the cFos induction (Figure 2H). We observed that the VMN^{PACAP} neurons efferently project to relatively few places in the brain, but the most prominent projections are in the POA. These projections particularly overlay in the caudal POA (Figure 2B, E), defined from +0.3 to −0.34 mm bregma, that are just lateral to the suprachiasmatic nucleus (SCN), above optic tract (OPT), but not in the traditional more

rostral (+0.6 to +0.3 mm bregma) regions required for stable body temperature. Besides the caudal POA, we also found VMN^{PACAP} projections in the BNST (Supplementary Figs. S2A–S2G), followed by lesser dense projections in the PVT (Supplementary Figs. S2H–S2K) and PAG (Supplementary Fig. S2L–S2R). We measured cFos induction at all the projection sites following IP CNO injection and compared them between PACAP^{hM3dq} mice (Figure 2D, G; Supplementary Figs. S2C, S2F, S2J, S2N, S2Q) and PACAP^{mCherry} control mice (Figure 2C, F; Supplementary Figs. S2B, S2E, S2I, S2M, S2P) and counted the cFos at each of these projection sites (Figure 2H; Supplementary Figs. S2D, S2G, S2K, S2O, S2R). We found that cFos in the PACAP^{hM3dq} mice were increased compared to the control mice in both sexes and at all projection sites.

Because the POA has been considered to be critical for energy expenditure and tissue thermogenesis [32–34] and this was the site where we observed the densest collection of synaptic terminals, we investigated whether the functional output of the VMN^{PACAP} neurons is at the caudal POA. We tested whether VMN^{PACAP} neurons directly activate cells in the caudal POA by measuring mini excitatory post-synaptic potential within neurons in the caudal POA following local stimulation of ChR2 in axonal terminals. For this, we unilaterally administered channelrhodopsin (ChR2) via *AAV$^{DIO\text{-}ChR2\text{-}eYFP}$* at the VMN of 8–12 weeks-old *Adcyap1^{Cre}* mice. ChR2 is expressed throughout the axon; thus, fiber optic light stimulation at the projection site will release vesicle pools from neurons that project to that site, but not from neurons that project elsewhere. Following sufficient time to induce expression of ChR2 throughout the neurons (4 weeks post-surgery), we performed electrophysiologic recording from neurons in apposition to ChR2-positive fibers using optogenetics, commonly referred to ChR2-assisted circuit mapping (CRACM) [35–37] (Figure 2I–J). We stimulated the VMN axonal inputs of these mice with blue light (490 nm) and recorded from the caudal POA (Figure 2I). Electrophysiological responses recorded in artificial cerebrospinal fluid (aCSF) alone revealed both excitatory and inhibitory currents following stimulation of VMN inputs (Figure 2J). Addition of glutamatergic blockers (CPP and NMQX 5 μM) eliminated both excitatory and inhibitory responses, which inhibits that VMN inputs are excitatory and drive feed-forward inhibition of caudal POA neurons via activation of local inhibitory neurons (Figure 2J). The percentage of cells activated and/or inhibited at either caudal POA or SCN (control region) were calculated in both sexes of mice (Figure 2K). We found that in both sexes of mice, VMN stimulation evoked both excitatory and inhibitory responses at caudal POA (11 of 14 neurons in males; 4 of 6 neurons in females). In males, 3 out 14 recorded caudal POA neurons did not respond to optogenetic stimulation of VMN inputs in slices where responses in other neurons were detected (Figure 2K). In females, one caudal POA neuron displayed only an inhibitory response to VMN stimulation with one other neuron showing no response (Figure 2K). Minimal responses were measured in SCN neurons following VMN input stimulation. Only 1 in 5 SCN neurons in male mice displayed both excitatory and inhibitory responses with the remaining 4 neurons showing no response (Figure 2K). In females, 2 out of 4 SCN neurons responded to VMN stimulation; one producing only an excitatory response with the other producing only an inhibitory response (Figure 2K).

3.3. Activating VMN^{PACAP} → caudal POA signaling induces tissue thermogenesis in both sexes of mice

We next tested the functional role for VMN^{PACAP} projections to the caudal POA and used the BNST as a control, given that projections from the VMN potently stimulate hyperglycemia which could be the mechanistic explanation for increasing energy expenditure and thermogenesis. For this we unilaterally administered *AAV$^{DIO\text{-}ChR2\text{-}eYFP}$* at the VMN of 8–12 weeks-old *Adcyap1^{Cre}* mice, combined sexes, as previously described [13,23,24] and implanted optical fiber (optrode) at either the caudal POA efferents or the BNST efferents as well as at the VMN somas (Figure 3A–B), to stimulate the optrodes using blue light to activate the ChR2 that was expressed along the axon and terminals of the VMN neurons. Additionally, we implanted temperature-sensing microchips at iBAT and iWAT. Following sufficient time to induce expression of ChR2 throughout the neurons (4 weeks post-surgery), we began the experiments. We measured temperature at iBAT (Figure 3C,F, 3I) and iWAT (Figure 3D,G, 3J) and blood glucose (Figure 3E,H, 3K) over the course of 2 h following the onset of blue light flash into the optrodes. We ran each experiment two times: once with blue light on and once with no blue light and the treatments were flipped for the experiments. Activating VMN^{PACAP} somas containing ChR2, via blue light, increased iBAT (Figure 3C) and iWAT (Figure 3D) temperature by 1 °C and 0.5 °C respectively and blood glucose by ∼10 mg/dL compared to the no blue light stimulation control. Blue light stimulation of the efferents containing ChR2 at the caudal POA, showed a similar increase in iBAT (Figure 3F) and iWAT (Figure 3G) temperature as well as blood glucose (Figure 3H) compared to the no light stimulation control. However, blue light stimulation of the efferents containing ChR2 at the BNST did not show a change in temperature at iBAT (Figure 3I) or iWAT (Figure 3J) but elevated blood glucose (Figure 3K) compared to the control.

3.4. After 24 h fasting, activation of VMN^{PACAP} → caudal POA signaling restores thermogenic activity in both sexes of mice

We then tested the effect of dietary signals and changes to feeding conditions on VMN^{PACAP} → caudal POA signaling and its thermogenic control. Importantly fasting reduces thermogenesis in adipose tissue depots, which could also suppress the ability for VMN^{PACAP} neurons to induce thermogenesis, but VMN^{PACAP} could also be effective at inducing thermogenesis when suppressed during negative energy balance. *Adcyap1^{ChR2}* mice from the previous set of optogenetics experiment in Section 3.3, were fasted for 24 h and then tested to determine if suppression of thermogenesis due to fasting can be overridden by activating these projections (Figure 4A). We measured temperature at iBAT (Figure 4B,E, 4H) and iWAT (Figure 4C,F, 4I) and blood glucose (Figure 4D,G, 4J) over the course of 2 h following the onset of blue light flash into the optrodes. We ran each experiment 3 times: (1) before fasting began with blue light off, (2) after 24-hour fasting with blue light on and (3) after 24-hour fasting with blue light off, and the treatments were flipped for the experiments. 24-hour fasting led to a drop in iBAT temperature (Figure 4B,E, 4H), iWAT temperature (Figure 4C,F, 4I) and blood glucose levels (Figure 4D,G, 4J) in the mice compared to the pre-fasting levels (control). Activating VMN^{PACAP} somas containing ChR2, via blue light, restored iBAT temperature (Figure 4B) and blood glucose (Figure 4D) to pre-fasting levels, however iWAT temperature (Figure 4C) was not restored. Blue light stimulation of the efferents containing ChR2 at the caudal POA, showed a restoration of both iBAT (Figure 4E) and iWAT (Figure 4F) temperatures but not blood glucose (Figure 4G) compared pre-fasting levels. In contrast, blue light stimulation of the efferents containing ChR2 at the BNST did not restore iBAT (Figure 4H) or iWAT (Figure 4I) temperatures but restored blood glucose level (Figure 4J) to pre-fasting levels.

To eliminate the possibility that ChR2 expression or the blue light itself is leading to any unwanted physiological effects, we administered *AAV$^{DIO\text{-}\ eGFP}$* at the VMN of a separate cohort of 8–12 weeks-old *Adcyap1^{Cre}* mice, combined sexes and performed identical

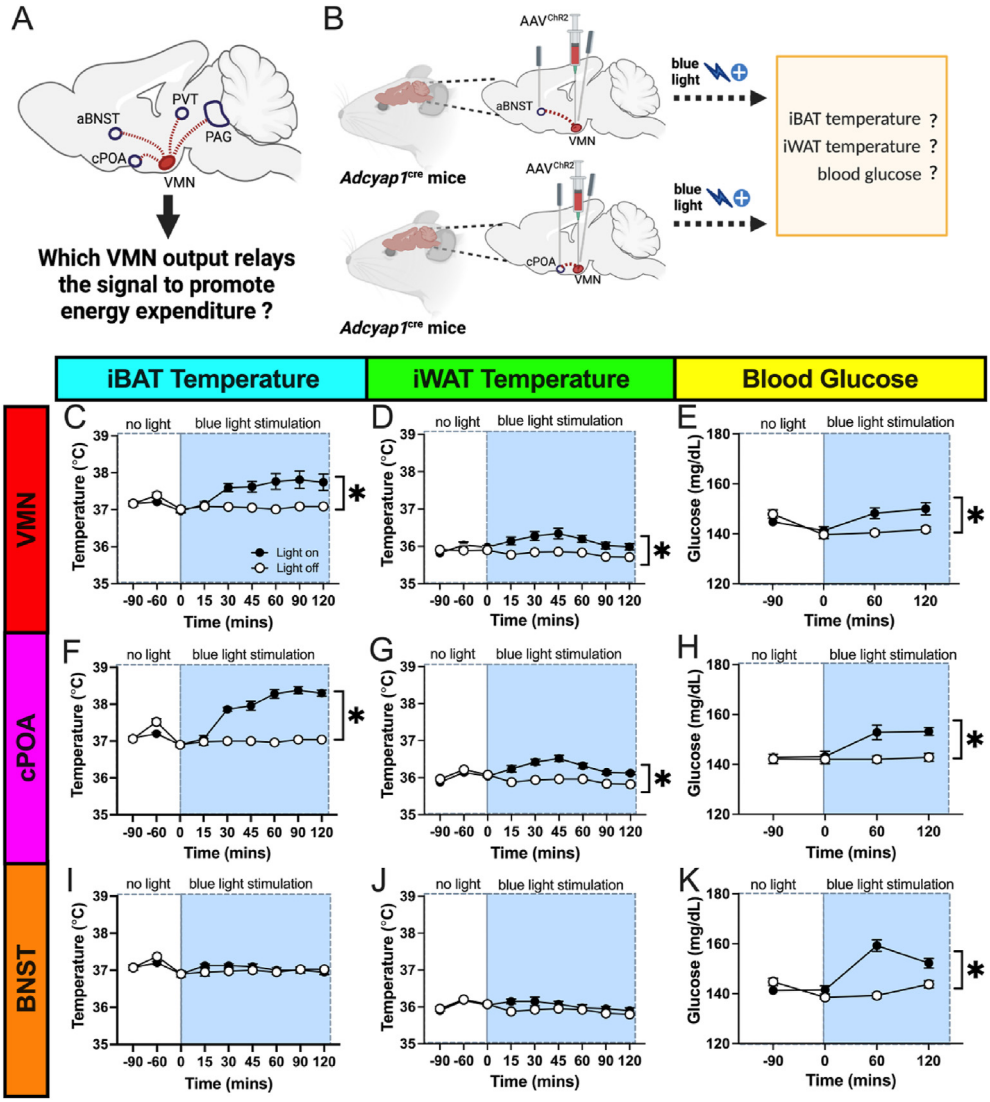

Figure 3: Activating VMN^{PACAP} → caudal POA signaling induces tissue thermogenesis in both sexes of mice. To test functional output of VMN^{PACAP} neurons (A), we introduced *AAV$^{DIO\text{-}ChR2\text{-}eYFP}$* in *Adcyap1^{Cre}* mice and implanted optrodes at VMN somas as well as at either caudal POA efferents or BNST efferents (B) and temperature microchips at iBAT and iWAT. To activate VMN^{PACAP} neurons at either cell body (C–E), caudal POA efferents (F–H), or BNST efferents (I–K), we stimulated either of the optrodes with blue light for 2 h and measured temperature above iBAT (C–I) and iWAT (D–J) and blood glucose (E–K). Data expressed as mean ± SEM and analyzed by two-way RM ANOVA, N = 7–14, *$p < 0.05$.

optogenetics experiment as discussed above. We ran each experiment 4 times: (1) before fasting began with blue light on, (2) before fasting began with no blue light, (3) after 24-hour fasting with blue light on and (4) after 24-hour fasting with no blue light, and the treatments were flipped for the experiments. Blue light stimulation of the efferents at the caudal POA after 24-hour fasting, showed no change in iBAT (Supplementary Fig. S3A) or iWAT (Supplementary Fig. S3B) temperatures or blood glucose levels (Supplementary Fig. S3C) compared pre-fasting levels. Similarly, blue light stimulation of the efferents at the BNST showed no difference in iBAT (Supplementary Fig. S3D) or iWAT (Supplementary Fig. S3E) temperatures or blood glucose level (Supplementary Fig. S3F) compared to pre-fasting levels. Also, when temperatures at iBAT or iWAT and blood glucose levels were compared between similar groups with blue light on versus groups with blue light off, no difference was found.

In summary, these data indicate that VMN^{PACAP} → caudal POA connection is necessary for tight thermogenic control when feeding conditions change. All these together indicate, VMN^{PACAP}, as well as associated signaling targets, are critical components to the control of energy balance by activating energy expenditure that impact adipose tissue function.

3.5. Acute activation of VMN^{PACAP} → caudal POA neurons induces distinct molecular programs within brown and beige adipose tissue in both sexes of mice

We next investigated how the VMN^{PACAP} → caudal POA signaling affects the molecular programs within the iBAT and iWAT. We administered *AAV$^{DIO\text{-}ChR2\text{-}eGFP}$* at the VMN of 8–12 weeks-old *Adcyap1^{Cre}* mice, combined sexes, in a separate cohort of mice, as described in Section 3.3, and implanted optrodes at the caudal POA

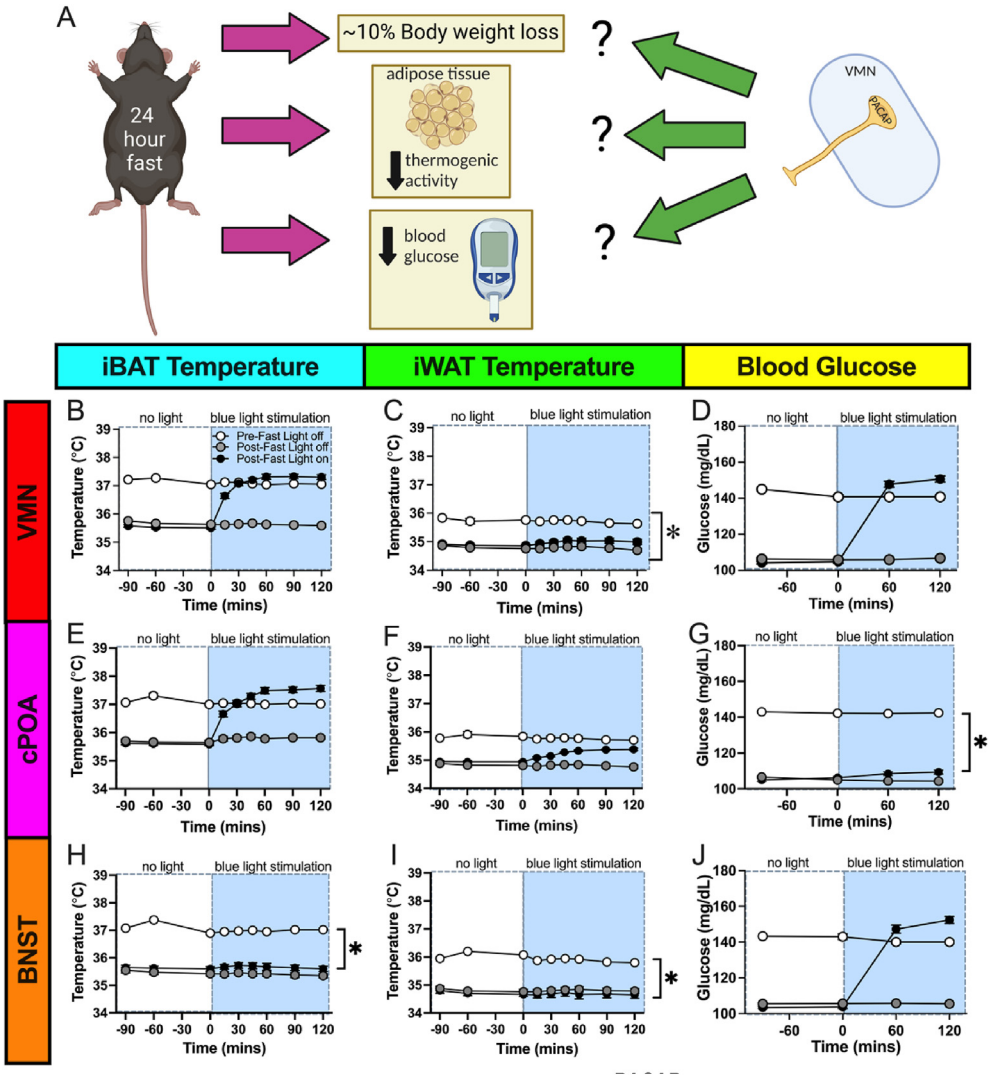

Figure 4: After 24 h fasting, activation of VMN^{PACAP} → caudal POA neurons restores thermogenic activity in both sexes of mice. In *Adcyap1*^{Cre} mice, we introduced *AAV*$^{DIO\text{-}ChR2\text{-}eYFP}$ and implanted optrodes at VMN somas as well as at either caudal POA efferents or BNST efferents and temperature microchips at iBAT and iWAT. Then, we subjected the mice to blue light stimulation or without blue light stimulation for 2 h to test the potential for *Adcyap1* neurons to impact brown and beige fat thermogenesis during fasting to restore normal levels of thermogenesis (A). We fasted the mice from Figure 4 for 24 h and then stimulated either at VMN somas (B–D), caudal POA efferents (E–G), or BNST efferents (H–J) with blue light for 2 h and measured temperature above iBAT (B,E,H) and iWAT (C, F, I) temperature and blood glucose (D–J). All data expressed as mean ± SEM and analyzed by two-way RM ANOVA. N = 7–14 mixed male and female mice. *$p < 0.05$.

efferents. Then, we subjected them to blue light stimulation or without blue light stimulation for 2-hours and tested them for temperatures at iBAT and iWAT, as described in sections 3.4 and 3.5, and then the iBAT and iWAT harvested from the mice after anesthesia, prior to transcardial perfusion. Total RNA from the iBAT and iWAT was isolated and sequenced. Total RNA-sequencing (RNA-seq) analysis (Figure 5A) was performed in the iBAT (Figure 5B–E) and iWAT (Figure 5F–I) of these mice 6 weeks after viral injection. Functional enrichment analysis, also called gene set analysis (GSA), was performed in iBAT (Figure 5D–E) and iWAT (Figure 5H–I) to discover biological annotations that are upregulated (Figure 5D, H) or downregulated (Figure 5E, I), within the list of top 20 differentially expressed genes (Figure 5B–C, 5F-5G). Comparison between molecular mechanisms and biological processes that are associated with mice with blue light stimulation versus control mice without blue light stimulation. In iBAT, we found molecular mechanisms contributing to the mitochondrial electron transport chain and cellular proliferation to be upregulated (Figure 5D) whereas molecular mechanisms aiding in lipid metabolism and cellular structural organization and protein post-translational modification/degradation pathways were downregulated (Figure 5E). However, in iWAT, we found the pathways facilitating nuclear and cellular restructure and remodeling to be upregulated (Figure 5H), while some downregulation in molecular pathways contributes to cell differentiation (Figure 5I). We also validated the top 3 hits from the RNA-sequencing analysis, using qRT-PCR of iBAT (Supplementary Fig. S4A) or iWAT (Supplementary Fig. S4B). We found *Ppt1*, *Kdm6b* to be upregulated in

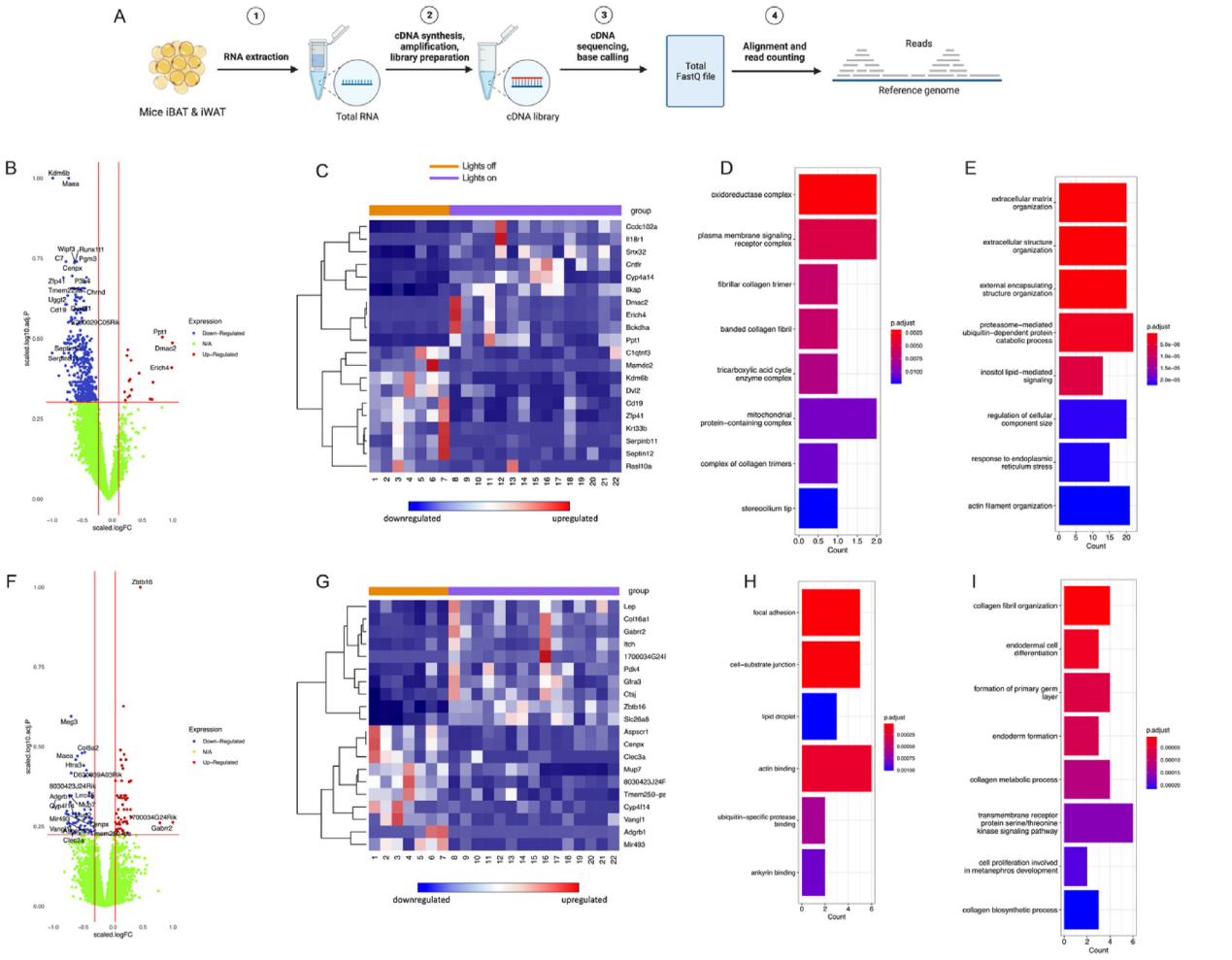

Figure 5: Acute activation of VMN^{PACAP} → caudal POA neurons induces distinct molecular programs in brown and beige adipose tissue in both sexes of mice. In *Adcyap1^{Cre}* mice, we introduced *AAV$^{DIO\text{-}ChR2\text{-}eYFP}$* and implanted optrodes at VMN somas and at either caudal POA efferents or BNST efferents and temperature microchips at iBAT and iWAT. Then, we subjected the mice to blue light stimulation or without blue light stimulation for 2 h and then the iBAT and iWAT were harvested from the mice after anesthesia, prior to transcardial perfusion. We then isolated total RNA from the iBAT and iWAT and performed total RNA-sequencing (A) of iBAT and iWAT isolated from mice after acute activation of VMN^{PACAP} → caudal POA neurons using optogenetics. Volcano plots (B,F), heatmaps (C,G) and functional enrichment plots with upregulated genes (D,H) and downregulated genes (E,I) from iBAT (B–E) and iWAT (F–I) were generated. N = 12–14 mixed male and female mice.

iBAT and *Zbtb16* and *Slc26a8* to be upregulated in iWAT, whereas the gene *MaeA* was downregulated in both iBAT and iWAT, confirming what we found in the RNA-sequencing results.

3.6. Activation of the of VMN^{PACAP} neurons at the caudal POA only leads to cFos induction at the POA and not other sites that VMN^{PACAP} neurons project to

We then tested whether activation of VMN^{PACAP} neurons' efferents at caudal POA, and not any other collateral nuclei like the BNST, PVT or PAG, are responsible for tissue thermogenesis at iBAT and iWAT in mice. Since, cFos induction is a marker of neuronal activation, we first observed projections (Figure 6A,D, 6G, 6K, 6N) from the VMN^{PACAP} neurons *AAV$^{DIO\text{-}syn\text{-}mRuby}$* at the VMN of 8–12 weeks-old *Adcyap1^{Cre}* mice to identify where the terminals are most concentrated in the brain. Then using brain sections from *Adcyap1^{Cre}* mice included in aforementioned experiments (as described in Sections 3.3, 3.4 And 3.5) and counted cFos (Figure 6B, E, L, O) in all those nuclei where the VMN^{PACAP} neurons projected to, i.e., caudal POA, BNST, PVT and PAG and compared them. We counted cFos induction in the mice with blue light stimulation (light on) and compared them with the group with no blue light stimulation (light off) (Figure 6C,F, I, J, M, P, Q). We also compared cFos induction between the contralateral (in relation to side with unilateral AAV injection and optrode placement) and ipsilateral sides of the mice with blue light stimulation (light on) (Figure 6C,F, I, J, M, P, Q). We found that blue light stimulation (light on) at VMN lead to increased cFos induction when compared to the light off group (Figure 6C, left) as well as the ipsilateral sides when compared to the contralateral sides (Figure 6C, right) of the mice that received blue light stimulation (light on). Blue light stimulation (light on) at the caudal POA lead to a similar increase in cFos induction when compared to the light off group (Figure 6F, left) and a similar increase on the ipsilateral sides when compared to the contralateral sides (Figure 6F, right) of the mice that received blue light stimulation (light on). On the contrary when we counted cFos induction at BNST (Figure 6H) and measured cFos at both the dorsal BNST (Figure 6I) and ventral BNST (Figure 6J) after blue light stimulation (light on) of that node, we did not see a significant change in the cFos induction when compared to the light off group (Figure 6I, left) and neither did we find any significant change in the cFos

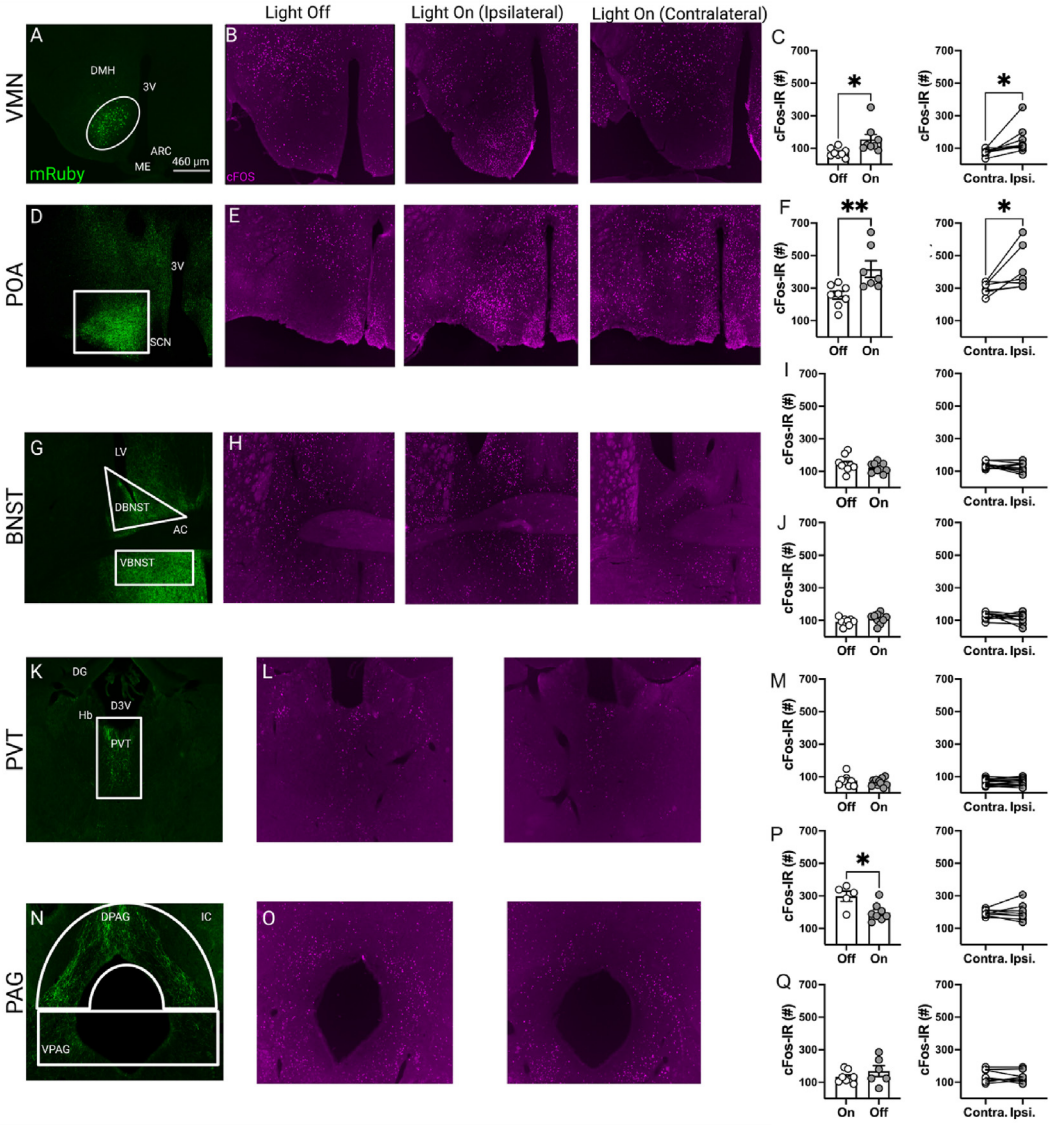

Figure 6: Activation of the of VMN^{PACAP} neurons at the caudal POA only leads to cFos induction at the POA and not other sites that VMN^{PACAP} neurons project to. We took brain sections from *Adcyap1*^{Cre} mice included in the aforementioned experiments (Figures 3–5) and stained for mRuby and also for cFos separately. Representative images showing mRuby at VMN (A), POA (D), BNST(G), PVT (K), PAG (N). Representative images showing cFos induction during 3 different conditions: (1) light off (left panels of B, E, H, L, O), (2) light on and ipsilateral side (middle panels of B, E, H, L, O) and (3) light on and contralateral side (right panels of B, E, H, L, O). The cFos was observed at VMN (B) and all the projection sites after blue light stimulation: at POA (E), BNST (H), PVT (L), PAG (O) and counted. The cFos induction at each region was counted and compared: VMN (C), POA (F), dorsal BNST (I), ventral BNST (J), PVT (M), dorsal PAG (P), ventral PAG (Q) and compared between the light off versus light on groups (left panels of C, F, I, J, M, P, Q) and between the contralateral (light on) versus ipsilateral (light on) groups (right panels of C, F, I, J, M, P, Q). In the representative images of cFos counts for PVT (L) and PAG (O), the contralateral and ipsilateral sides are represented together in one image, with the left side of the images showing the ipsilateral side and the right side showing the contralateral side. N = 6–10 mice. Scalebar = 460 µm (A, D, G, K, N) and 180 µm (B, E, H, L, O). LV = Lateral ventricle. 3V = 3rd ventricle. AC = Anterior commissure. DBNST = Dorsal bed nucleus of stria terminalis. VBNST = Ventral bed nucleus of stria terminalis. DG = Dentate gyrus. D3V = Dorsal 3rd ventricle. Hb = Habenular commissure. PVT = Paraventricular thalamus. DPAG = Dorsal periaqueductal gray. VPAG = Ventral periaqueductal gray. IC = Inferior colliculus. Aq = Aqueduct. Data expressed as mean ± SEM and analyzed by student's t test (left and right panels of C, F, I, J, M, P, Q), *$p < 0.05$, **$p < 0.01$.

induction when the ipsilateral sides were compared to the contralateral sides (Figure 6I, right) of the mice that received blue light stimulation (light on). We also did not find any significant change in the cFos induction at PVT (Figure 6L) when comparing light on and light off groups (Figure 6M, left) or the contralateral versus ipsilateral sides (Figure 6M, right) of the mice that received blue light stimulation (light on). When measuring activity at PAG (Figure 6O), we found that blue light stimulation (light on) at VMN lead to increased cFos induction at dorsal PAG when compared to the light off group (Figure 6P, left) as well as the ipsilateral sides when compared to the contralateral sides (Figure 6P, right) of the mice that received blue light stimulation (light on). But the at the ventral PAG there was no significant change in cFos induction when comparing light on and light off groups (Figure 6Q, left) or the contralateral versus ipsilateral sides (Figure 6Q, right) of the mice that received blue light stimulation (light on). These results validated that, activation of VMN^{PACAP} neurons' efferents at caudal POA, and not any other collateral nuclei, are responsible for tissue thermogenesis at iBAT and iWAT in mice.

3.7. The induction of tissue thermogenesis by VMN^{PACAP} → caudal POA neurons is blocked by inhibition of neurons within the caudal POA

We then tested whether activation of VMN^{PACAP} → caudal POA neurons, indeed, is necessary for tissue thermogenesis at iBAT and iWAT in mice, we activated the VMN^{PACAP} neurons while inhibiting the caudal POA neurons and studied the effect on iBAT and iWAT temperatures in both sexes of mice. For this, we unilaterally administered *AAV$^{DIO\text{-}ChR2\text{-}eYFP}$* at the VMN and *AAV$^{hM4Di\text{-}mCherry}$* at the caudal POA of 8–12 weeks-old *Adcyap1^{Cre}* mice, combined sexes, as previously described [13,23,24] to induce cre-dependent expression of ChR2 at the VMN and cre-independent expression of hM4Di at the caudal POA (Figure 7A). We also, implanted an optical fiber (optrode) at the caudal POA efferents (Figure 7A). This was done to stimulate the optrode using blue light to activate the ChR2 that was expressed along the axon and terminals of the VMN neurons and concurrently the inhibit the neurons at the caudal POA via CNO IP injection, where the CNO will work on the hM4Di receptors expressed in the caudal POA neurons. Additionally, we implanted temperature-sensing microchips at iBAT and iWAT. Following sufficient time to induce expression of cre-dependent ChR2 and cre-independent hM4Di throughout the VMN and caudal POA neurons respectively (4 weeks post-surgery), we began the experiments. We measured temperature at iBAT (Figure 7B,C, 7D) and iWAT (Figure 7E,F,7G) over the course of 2 h following the onset of blue light flash into the optrodes. We ran each experiment four times: with blue light on or with no blue light as well as with IP CNO or saline administration and the treatments were flipped for the experiments. Blue light stimulation of the VMN^{PACAP} efferents containing ChR2 at the caudal POA along with IP saline administration, increased iBAT (Figure 7B, C) by 1 °C and with no change in iWAT (Figure 7D, E) temperature, compared to the no blue light stimulation control. Whereas when the blue light stimulation, to activate VMN^{PACAP} efferents containing ChR2 at the caudal POA, was combined with the IP CNO administration, to inhibit the hM4Di expressing caudal POA neurons, there was no increase in iBAT (Figure 7B, C) or iWAT (Figure 7D, E) temperature compared to the no blue light stimulation control.

3.8. Overall model

Together our data demonstrates that the subpopulation of VMN^{Sf1} neurons expressing the PACAP neuropeptide, projects to caudal POA and transmits the signal downstream to the periphery (Figure 8). These VMN neurons transmit the signal to the periphery to iBAT and iWAT via the preoptic outputs to increase thermogenesis and energy expenditure by means of mitochondrial uncoupling. While acute activation of this neurocircuit promotes thermogenesis at iBAT and induces mechanisms involved in browning, at iWAT; chronic activation of this circuit leads to elevated thermogenic programming in iBAT and iWAT which ultimately improves metabolization of excess energy resulting in weight loss.

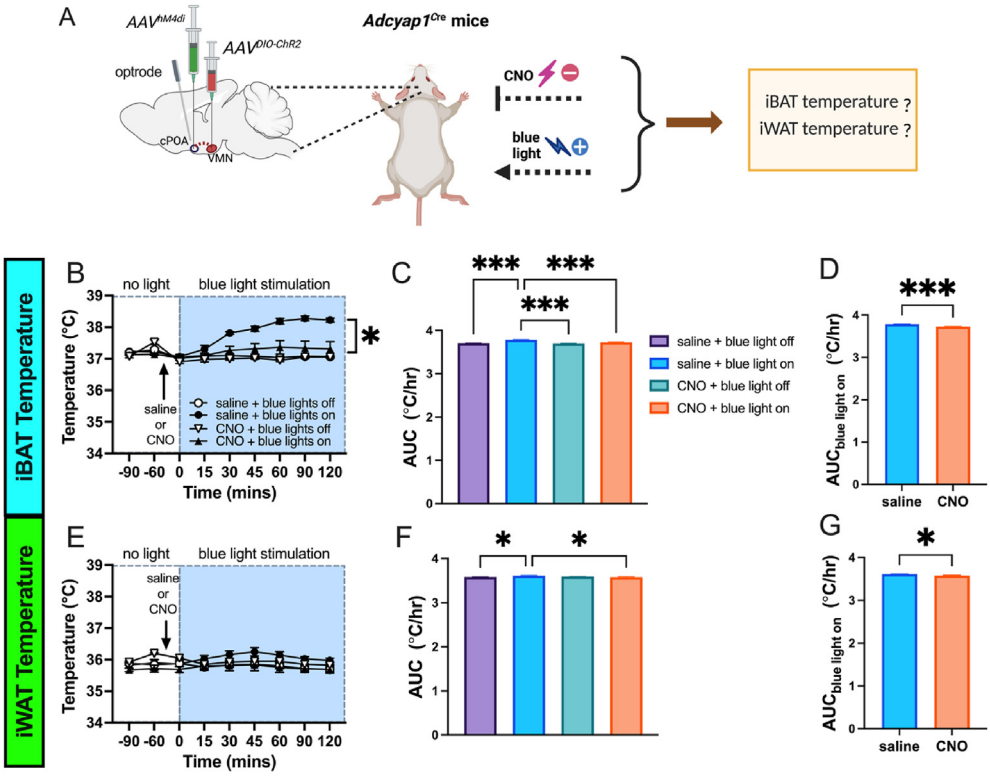

Figure 7: The induction of tissue thermogenesis by VMN^{PACAP} → caudal POA neurons is blocked by inhibition of neurons within the caudal POA. We unilaterally administered *AAV$^{DIO\text{-}ChR2\text{-}eYFP}$* at the VMN and *AAV$^{hM4Di\text{-}mCherry}$* at the caudal POA of *Adcyap1^{Cre}* mice and implanted an optrode at the caudal POA efferents (A). We then measured iBAT (B) and iWAT (E) temperatures after activating the VMN^{PACAP} neurons while inhibiting the caudal POA neurons and compared the results between the groups. We also measured the area under the curve at iBAT (C) and iWAT (F) temperatures and compared between the different groups. We then separately compared area under the curve at iBAT (D) and iWAT (G) temperatures in the groups with blue light on and compared between IP saline with Ip CNO injection. N = 9 mixed male and female mice. Data expressed as mean ± SEM and analyzed by either two-way RM ANOVA (B, E), one-way ANOVA (C, F) or by student's t test (D, G). *p < 0.05, **p < 0.01, ***p < 0.0001.

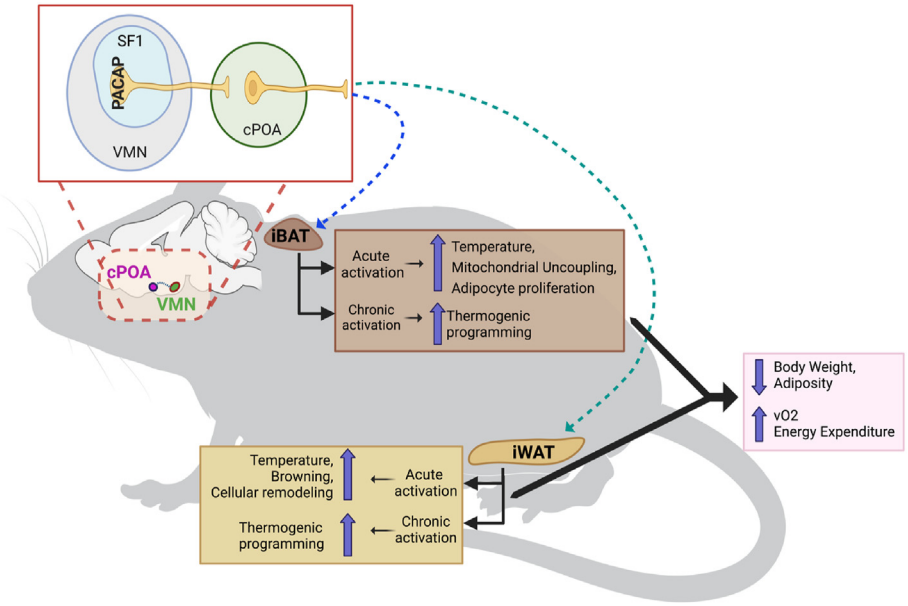

Figure 8: Overall model. Our data indicates that the subpopulation of VMN^{Sf1} neurons expressing the PACAP neuropeptide, projects to caudal POA. These VMN^{PACAP} neurons transmit distinct signals to the periphery to iBAT and iWAT via the caudal POA. Acute activation of this neurocircuit promotes distinct physiological mechanisms at iBAT and iWAT than what chronic activation of this circuit leads to. Together these mechanisms reduce body weight and adiposity and increase vO2 and energy expenditure.

4. DISCUSSION

Our data demonstrate that a subset of VMN neurons induce tissue thermogenesis via the POA, which can be activated to reduce obesity and increase energy expenditure in diet-induced obese male mice. Proper function and fine tuning of this neurocircuit is essential for the maintenance of energy balance via energy expenditure. Activation of this circuit increases temperature above both the brown and beige adipose depots and reduces adipose mass in diet-induced obese male mice. Together with historical data linking nutrient sensing with the ventromedial hypothalamus, our data support a model for this circuit is to elevate the metabolization of excess energy, when necessary, but not necessarily for the purpose of temperature control. In support of this notion, *Adcyap1* expression is reduced after both fasting and in *ob/ob* mice, which can each be restored by leptin administration [20]. Taken together with our data, PACAP regulation according to energy status signals is a key regulator of energy expenditure and for whole body energy balance. It remains to be seen if this circuit can be targeted for either body weight loss or normalizing energy expenditure in negative energy balance conditions.

Our findings are consistent with the view that there is a subset of VMN cells that are essential in controlling tissue thermogenesis and energy expenditure. Our data would provide further support that the key subset contains the neuropeptide PACAP. Indeed, we extended upon data included in our previously published manuscript [16]. In our previous paper, we demonstrated that a VMN-centered PACAP knockout leads to obesity in both male and female mice, that only leads to a modest increase in food intake once the animals are obese [16]. Surprisingly, we only observed changes in glycemic responses after the mice had been obese for months, but not 3 weeks as they were developing the obesity phenotype. However, we observed suppressed energy expenditure during the early development of obesity. Also in this paper, we demonstrated that activating VMN^{PACAP} cells by DREADD-hM3dq induction induced BAT thermogenesis. We now both reproduced that finding using ChR2-mediated activation and also demonstrated that these cells have the potential to also stimulate iWAT thermogenesis. These thermogenic functions are most effective during negative energy balance. Taken together with previous evidence that fasting and loss of leptin signaling reduces *Adcyap1* expression, these data demonstrate the potential for this circuit to override suppressed energy expenditure during periods of negative energy balance to metabolize excess nutrients when necessary via thermogenic signaling pathways. More investigation is needed to examine the contexts in which this circuit is recruited. While gene expression data suggests that this circuit is activated in energy balance excess and suppressed in negative energy balance, more data is needed. Additionally, there may be other signals that could impact the function of this circuit, including cold temperature.

Originally, it was assumed that energy expenditure stimulating VMN cells act via caudally projecting brainstem mechanisms [38], but the recent evidence using viral tracers has been lacking [18,19]. Thus, VMN cells are more likely to be present further upstream in energy expenditure-controlling circuits than previously assumed. We and others have demonstrated that there are no projections into the key brain areas that control adipose tissue and muscle function [18,19,39]. Furthermore, projections into the periaqueductal gray potently induce defensive behaviors, which is a shared function of the VMN and the periaqueductal gray [40]. Thus, there must be an alternative output that the VMN activates as part of the essential circuit for energy expenditure stimulation by the VMN. Indeed, the VMN sends robust projections to the caudal POA, as we describe, which is a region in temperature control and locomotor activity. Induction of thermogenesis through the POA likely involves activation of the sympathetic nervous activity. Denervation of the BAT depletes UCP1 from adipocytes, reduces thermogenesis, leads to cold intolerance, and increases susceptibility to obesity [33,41–43] Furthermore, optogenetic activation of tyrosine-hydroxylase nerves in BAT induces a very similar rise in BAT temperature from what we observed in our study and involves temperature-responsive pathways through the POA [33,44]. VMN^{PACAP} cells could engage these mechanisms that activate responses to cold

and warm temperature or potentially a separate set of cells that don't directly control temperature but instead elevate metabolism in peripheral tissues via thermogenic pathways. Future studies will tease out the mechanisms by which the POA controls this function.

However, VMN^{PACAP} neurons are not a segregated population of VMN neurons and are expressed throughout the nucleus, but particularly in the dorsomedial division of the VMN. Other studies have demonstrated that many VMN neurons are glucose-responsive, but our data would support VMN^{PACAP} neurons do not primarily control blood glucose because the induction of hyperglycemia by activating VMN^{PACAP} neurons is not as robust VMN^{Sf1} neurons, or the subset of VMN neurons that contain the cholecystokinin-b receptor [13,19]. Indeed, we observe that the primary output from VMN^{PACAP} neurons is not the BNST, which is the output that VMN^{Sf1} neurons and VMN^{NOS1} neurons (expressing nitric oxide synthase 1) act via to mobilize blood glucose. While VMN^{PACAP} neurons may be glucose-responsive, the responsiveness to blood glucose may instead tune tissue thermogenesis in adipose tissue. Although, there may just be a small subset of VMN^{PACAP} neurons that participate in the counterregulatory response to hypoglycemia intermingled with those that control energy expenditure.

There could be other functions for VMN^{PACAP} → caudal POA signaling. For instance, chronic activation may reveal effects outside of thermogenesis. Indeed, a recent study demonstrated that chronic activation of VMN^{Sf1} neurons reduced inflammatory markers within adipose tissue in diet-induced obese mice [45]. While this study focused on more acute signaling for thermogenesis, we could be missing long term effects for this circuit that could benefit the individual. In addition to other functions for this circuit, other important VMN functions are likely primarily driven by separate VMN cells. While we did observe an increase in blood glucose after activating projections to the BNST, this is much more modest than what has been observed with other VMN subpopulations [13,18,19]. However, continuous induction of thermogenic pathways in the adipose tissue could also impact lipid trafficking and glucose transport, which could have beneficial effects in diabetes and obesity. In addition, separate VMN cells induce stress and anxiety behaviors, which we did observe in the *Sf1^{Cre}* mice, but not in the *Adcyap1^{Cre}* mice. This likely is through a separate output, which is most likely the periaqueductal gray. However, the paraventricular thalamus has also been implicated in these functions and may serve another role, which could lead to anorexia upon activation [20]. More investigation is needed to define the output circuits from the VMN in all the functions related to the nucleus.

Our RNA-sequencing analysis of the iBAT and iWAT showed that acute activation (2 h of stimulation) of VMN^{PACAP} → caudal POA signaling engages molecular mechanisms that ultimately contribute, at least in part, to thermogenesis and improved energy metabolism. Importantly, canonical thermogenic genes are not among our most differentially expressed genes in either iBAT or iWAT, likely due to the acute nature of the study only at 2 h, mainly because thermogenic programming in adipose tissue typically occurs with stimulation over the course of days, (as we saw in our study of *Adcyap1^{VMN}KO*). The most differentially upregulated genes in iBAT (Supplementary Fig. S6A): *Ppt1*, *Kdm6b* are involved in facilitating energy metabolism. *Ppt1* is known to be encoding an enzyme responsible for hydrolyzing long chain fatty acids from lysosomal cargo and interacts with the mitochondrial F_1 ATP-synthase [46] but its role in energy metabolism has not been explored. Since lysosomes can sense nutrient availability depending on their cargo storage and regulate energy metabolism [47], we speculate that *Ppt1* contributes to regulation of energy metabolism as well. The gene *Kdm6b* encodes the protein KDM6B which facilitates browning of iWAT [48,49]. In iWAT, the most differentially upregulated genes (Supplementary Fig. S6B): *Zbtb16* and *Slc26a8* are also found to be involved in induction of mitochondrial metabolism and uncoupling capacity. *Zbtb16* is a significant energy metabolism modulator and overexpression of the gene has been found to induce thermogenic programming including induction of mitochondrial fatty acid oxidation and uncoupling/electron transport chain [50,51]. The *Slc26a8* gene is known to stimulate anion transport activity of the cystic fibrosis transmembrane conductance regulator (CFTR) which in turn facilitates ATP synthesis, ATP transport, and influences energy expenditure by regulating nutrient absorption and digestion [52,53]. The gene *MaeA* was found to be most differentially downregulated in both iBAT and iWAT. The protein MaeA is an E3 ubiquitin ligase subunit and is essential for maintenance of hematopoietic stem cells (HSCs) and autophagy [54]. Its role in energy expenditure or metabolism has not been explored much, but since studies show that loss of E3 ubiquitin ligase leads to impaired nutrient sensing and metabolism in peripheral tissues [55], MaeA may have an important role to play in control of energy expenditure, especially in presence to dietary signals. These findings together with the GSA result indicate that acute activation of the VMN^{PACAP} → caudal POA circuit leads to a distinct genetic program within each the brown and the beige adipose depots, that together are critical for the maintenance of energy balance. Adipose tissue is highly plastic with a high capacity for remodeling between iBAT to iWAT to pgWAT and vice-versa, in terms of metabolic and thermogenic activity, depending on the hormonal or environmental stimuli [56–60]. Future studies will determine the role of increased proliferation and mitochondrial uncoupling in the brown adipocytes in iBAT and cellular remodeling in iWAT on metabolic health.

Here we also validated that the projections from VMN^{PACAP} neurons that lie at the caudal POA are indeed necessary for inducing adipose tissue thermogenesis. Acute neuronal activation at the different VMN^{PACAP} neurons' efferents indicated the importance of the VMN^{PACAP} → caudal POA signaling in eliciting thermogenesis. This combined with the fact that inhibition of the caudal POA neurons even after activating the VMN^{PACAP} neurons' efferents at the caudal POA blunted the signaling mechanism that triggered adipose tissue thermogenesis response. However, in absence of the inhibition of caudal POA neurons, the thermogenic response was restored alone by the activation of the VMN^{PACAP} neurons' efferents at the caudal POA. At this time, we are unable to confirm that this is a direct connection between the VMN^{PACAP} and the caudal POA. Even though this is the most likely explanation, we cannot rule out that there is another neuron between the VMN and the caudal POA that is integral to the function of this circuit. But it is clear from our findings that the caudal POA signaling is necessary for VMN^{PACAP} cells to induce adipose tissue thermogenesis.

5. CONCLUSION

In all, we define the anatomical output that the VMN uses to stimulate energy expenditure, which is even more effective in negative energy balance to stimulate tissue thermogenesis. We demonstrate that the VMN can activate energy expenditure in diet-induced obese male mice to reduce adipose mass and increase energy expenditure. This effect is associated with an upregulation in the expression of key thermogenic markers in the brown adipose tissue. Lastly, we identify the differentially expressed genes in both brown and beige adipose tissue immediately following acute activation of VMN^{PACAP} neurons that project to the caudal POA and demonstrate that there are very different pathways activated that likely lead to the overall goal of stimulating energy expenditure. These findings will provide new avenues to target for future treatment of obesity.

SUPPORT

NIH R01DK136897, ADA 17-INI-15, Ralph W. and Grace M. Showalter Trust, IU CDMD Pilot and Feasibility Program, Indiana Biosciences Research Institute.

CREDIT AUTHORSHIP CONTRIBUTION STATEMENT

Rashmita Basu: Writing — review & editing, Writing — original draft, Visualization, Validation, Project administration, Methodology, Investigation, Formal analysis, Data curation, Conceptualization. **Andrew J. Elmendorf:** Writing — review & editing, Visualization, Validation, Methodology, Formal analysis, Data curation. **Betty Lorentz:** Writing — review & editing, Investigation, Formal analysis, Data curation. **Connor A. Mahler:** Writing — review & editing, Investigation, Formal analysis, Data curation. **Olivia Lazzaro:** Writing — review & editing, Formal analysis, Data curation. **Britany App:** Writing — review & editing, Investigation, Formal analysis, Data curation. **Shudi Zhou:** Writing — review & editing, Investigation, Formal analysis, Data curation. **Yura Yamamoto:** Investigation, Data curation. **Mya Suber:** Investigation, Data curation. **Jamie C. Wann:** Writing — review & editing, Investigation, Data curation. **Hyun Cheol Roh:** Writing — review & editing, Supervision, Resources, Methodology, Formal analysis, Data curation. **Patrick L. Sheets:** Writing — review & editing, Visualization, Validation, Supervision, Methodology, Investigation, Funding acquisition, Formal analysis, Data curation. **Travis S. Johnson:** Writing — review & editing, Validation, Supervision, Resources, Investigation, Formal analysis, Data curation. **Jonathan N. Flak:** Writing — review & editing, Writing — original draft, Visualization, Validation, Supervision, Resources, Project administration, Methodology, Investigation, Funding acquisition, Formal analysis, Data curation, Conceptualization.

ACKNOWLEDGEMENTS

We thank Indiana University School of Medicine Center for Medical Genomics, Center for Computational Biology and Bioinformatics, Laboratory Animal Resource Center and Metabolic Phenotypic Centre. We also thank members of the Indiana University School of Medicine Center for Diabetes and Metabolic Disease, Department of Pharmacology and Toxicology and the Lilly Diabetes Research Center at Indiana Biosciences Research Institute for helpful discussions and guidance. Research support was provided by Pathway 17-INI-15, IU CDMD (United States) Pilot and Feasibility Program, Showalter Trust, The Eli Lilly (United States) LRAP Program, The Indiana Biosciences Research Institute, and. All the graphical art was created using Biorender.com (United States).

DECLARATION OF COMPETING INTEREST

Jonathan N. Flak and Travis S. Johnson have received research support from Eli Lilly and Company, United States for separate projects in their respective laboratories.

DATA AVAILABILITY

Data will be made available on request.

APPENDIX A. SUPPLEMENTARY DATA

Supplementary data to this article can be found online at https://doi.org/10.1016/j.molmet.2024.101951.

REFERENCES

[1] Ogden CL, Yanovski SZ, Carroll MD, Flegal KM. The epidemiology of obesity. Gastroenterology 2007;132(6):2087—102.
[2] Tran LT, Park S, Kim SK, Lee JS, Kim KW, Kwon O. Hypothalamic control of energy expenditure and thermogenesis. Exp Mol Med 2022;54(4):358—69.
[3] Schwartz MW, Porte Jr D. Diabetes, obesity, and the brain. Science 2005;307(5708):375—9.
[4] Cannon B, Nedergaard J. Nonshivering thermogenesis and its adequate measurement in metabolic studies. J Exp Biol 2011;214(Pt 2):242—53.
[5] Wu J, Jun H, McDermott JR. Formation and activation of thermogenic fat. Trends Genet 2015;31(5):232—8.
[6] Berg T, Jensen J. Tyramine reveals failing alpha2-adrenoceptor control of catecholamine release and total peripheral vascular resistance in hypertensive rats. Front Neurol 2013;4:19.
[7] Tseng YH, Cypess AM, Kahn CR. Cellular bioenergetics as a target for obesity therapy. Nat Rev Drug Discov 2010;9(6):465—82.
[8] Leblanc J, Dussault J, Lupien D, Richard D. Effect of diet and exercise on norepinephrine-induced thermogenesis in male and female rats. J Appl Physiol Respir Environ Exerc Physiol 1982;52(3):556—61.
[9] Yu S, Qualls-Creekmore E, Rezai-Zadeh K, Jiang Y, Berthoud HR, Morrison CD, et al. Glutamatergic preoptic area neurons that express leptin receptors drive temperature-dependent body weight homeostasis. J Neurosci 2016;36(18):5034—46.
[10] Adjeitey CN, Mailloux RJ, Dekemp RA, Harper ME. Mitochondrial uncoupling in skeletal muscle by UCP1 augments energy expenditure and glutathione content while mitigating ROS production. Am J Physiol Endocrinol Metab 2013;305(3):E405—15.
[11] Roh E, Song DK, Kim MS. Emerging role of the brain in the homeostatic regulation of energy and glucose metabolism. Exp Mol Med 2016;48:e216.
[12] Seoane-Collazo P, Ferno J, Gonzalez F, Dieguez C, Leis R, Nogueiras R, et al. Hypothalamic-autonomic control of energy homeostasis. Endocrine 2015;50(2):276—91.
[13] Flak JN, Goforth P, Dell'Orco J, Sabatini PV, Li C, Bozadjieva N, et al. Ventromedial hypothalamic nucleus neuronal subset regulates blood glucose independently of insulin. J Clin Invest 2020;30(6):2943—52.
[14] Tanida M, Shintani N, Morita Y, Tsukiyama N, Hatanaka M, Hashimoto H, et al. Regulation of autonomic nerve activities by central pituitary adenylate cyclase-activating polypeptide. Regul Pept 2010;161(1—3):73—80.
[15] Tanida M, Hayata A, Shintani N, Yamamoto N, Kurata Y, Shibamoto T, et al. Central PACAP mediates the sympathetic effects of leptin in a tissue-specific manner. Neuroscience 2013;238:297—304.
[16] Bozadjieva-Kramer N, Ross RA, Johnson DQ, Fenselau H, Haggerty DL, Atwood B, et al. The role of mediobasal hypothalamic PACAP in the control of body weight and metabolism. Endocrinology 2021;162(4).
[17] Hawke Z, Ivanov TR, Bechtold DA, Dhillon H, Lowell BB, Luckman SM. PACAP neurons in the hypothalamic ventromedial nucleus are targets of central leptin signaling. J Neurosci 2009;29(47):14828—35.
[18] Faber CL, Matsen ME, Velasco KR, Damian V, Phan BA, Adam D, et al. Distinct neuronal projections from the hypothalamic ventromedial nucleus mediate glycemic and behavioral effects. Diabetes 2018;67(12):2518—29.
[19] Meek TH, Nelson JT, Matsen ME, Dorfman MD, Guyenet SJ, Damian V, et al. Functional identification of a neurocircuit regulating blood glucose. Proc Natl Acad Sci U S A 2016;113(14):E2073—82.
[20] Zhang J, Chen D, Sweeney P, Yang Y. An excitatory ventromedial hypothalamus to paraventricular thalamus circuit that suppresses food intake. Nat Commun 2020;11(1):6326.
[21] Dhillon H, Zigman JM, Ye C, Lee CE, McGovern RA, Tang V, et al. Leptin directly activates SF1 neurons in the VMH, and this action by leptin is required for normal body-weight homeostasis. Neuron 2006;49(2):191—203.

[22] Tan CL, Cooke EK, Leib DE, Lin YC, Daly GE, Zimmerman CA, et al. Warm-Sensitive neurons that control body temperature. Cell 2016;167(1):47–59 e15.
[23] Flak JN, Arble D, Pan W, Patterson C, Lanigan T, Goforth PB, et al. A leptin-regulated circuit controls glucose mobilization during noxious stimuli. J Clin Invest 2017;127(8):3103–13.
[24] Flak JN, Patterson CM, Garfield AS, D'Agostino G, Goforth PB, Sutton AK, et al. Leptin-inhibited PBN neurons enhance responses to hypoglycemia in negative energy balance. Nat Neurosci 2014;17(12):1744–50.
[25] Law CW, Chen Y, Shi W, Smyth GK. voom: precision weights unlock linear model analysis tools for RNA-seq read counts. Genome Biol 2014:15.
[26] Law CW, Alhamdoosh M, Su S, Dong X, Tian L, Smyth GK, et al. RNA-seq analysis is easy as 1-2-3 with limma, Glimma and edgeR. ISCB Communications Journal 2016;5(1408).
[27] Ritchie ME, Phipson B, Wu D, Hu Y, Law CW, Shi W, et al. Limma powers differential expression analyses for RNA-sequencing and microarray studies. Nucleic Acids Res 2015;43:e47.
[28] McCarthy GS. Ebayes: empirical Bayes statistics for differential expression. Limma: linear models for microarray data. 2020.
[29] Pagès H, Carlson M, Falcon S, Li N. AnnotationDbi: manipulation of SQLite-based annotations in bioconductor. 2021.
[30] Yu G. Enrichplot: visualization of functional enrichment result. 2022.
[31] Wickham H. ggplot2: elegant graphics for data analysis. New York: Springer-Verlag; 2016.
[32] Yu S, Francois M, Huesing C, Munzberg H. The hypothalamic preoptic area and body weight control. Neuroendocrinology 2018;106(2):187–94.
[33] Morrison SF, Madden CJ, Tupone D. Central neural regulation of brown adipose tissue thermogenesis and energy expenditure. Cell Metabol 2014;19(5):741–56.
[34] Clapham JC. Central control of thermogenesis. Neuropharmacology 2012;63(1):111–23.
[35] Cheriyan J, Kaushik MK, Ferreira AN, Sheets PL. Specific targeting of the basolateral amygdala to projectionally defined pyramidal neurons in prelimbic and infralimbic cortex. eNeuro 2016;3(2).
[36] Cheriyan J, Sheets PL. Peripheral nerve injury reduces the excitation-inhibition balance of basolateral amygdala inputs to prelimbic pyramidal neurons projecting to the periaqueductal gray. Mol Brain 2020;13(1):100.
[37] Li JN, Sheets PL. Spared nerve injury differentially alters parabrachial monosynaptic excitatory inputs to molecularly specific neurons in distinct subregions of the central amygdala. Pain 2020;161(1):166–76.
[38] Swanson LW, Kuypers HG. A direct projection from the ventromedial nucleus and retrochiasmatic area of the hypothalamus to the medulla and spinal cord of the rat. Neurosci Lett 1980;17(3):307–12.
[39] Sabatini PV, Wang J, Rupp AC, Affinati AH, Flak JN, Li C, et al. tTARGIT AAVs mediate the sensitive and flexible manipulation of intersectional neuronal populations in mice. Elife 2021;10.
[40] Wang L, Chen IZ, Lin D. Collateral pathways from the ventromedial hypothalamus mediate defensive behaviors. Neuron 2015;85(6):1344–58.
[41] Fischer AW, Schlein C, Cannon B, Heeren J, Nedergaard J. Intact innervation is essential for diet-induced recruitment of brown adipose tissue. Am J Physiol Endocrinol Metab 2019;316(3):E487–503.
[42] Lee YH, Petkova AP, Konkar AA, Granneman JG. Cellular origins of cold-induced brown adipocytes in adult mice. Faseb J 2015;29(1):286–99.
[43] Rondini EA, Mladenovic-Lucas L, Roush WR, Halvorsen GT, Green AE, Granneman JG. Novel pharmacological probes reveal ABHD5 as a locus of lipolysis control in white and Brown adipocytes. J Pharmacol Exp Therapeut 2017;363(3):367–76.
[44] Lyons CE, Razzoli M, Larson E, Svedberg D, Frontini A, Cinti S, et al. Optogenetic-induced sympathetic neuromodulation of brown adipose tissue thermogenesis. Faseb J 2020;34(2):2765–73.
[45] Rashid M, Kondoh K, Palfalvi G, Nakajima KI, Minokoshi Y. Inhibition of high-fat diet-induced inflammatory responses in adipose tissue by SF1-expressing neurons of the ventromedial hypothalamus. Cell Rep 2023;42(6):112627.
[46] Lyly A, Marjavaara SK, Kyttala A, Uusi-Rauva K, Luiro K, Kopra O, et al. Deficiency of the INCL protein Ppt1 results in changes in ectopic F1-ATP synthase and altered cholesterol metabolism. Hum Mol Genet 2008;17(10):1406–17.
[47] Settembre C, Fraldi A, Medina DL, Ballabio A. Signals from the lysosome: a control centre for cellular clearance and energy metabolism. Nat Rev Mol Cell Biol 2013;14(5):283–96.
[48] Gao W, Liu JL, Lu X, Yang Q. Epigenetic regulation of energy metabolism in obesity. J Mol Cell Biol 2021;13(7):480–99.
[49] Pan D, Huang L, Zhu LJ, Zou T, Ou J, Zhou W, et al. Jmjd3-Mediated H3K27me3 dynamics orchestrate Brown fat development and regulate white fat plasticity. Dev Cell 2015;35(5):568–83.
[50] Plaisier CL, Bennett BJ, He A, Guan B, Lusis AJ, Reue K, et al. Zbtb16 has a role in brown adipocyte bioenergetics. Nutr Diabetes 2012;2(9):e46.
[51] Skolnikova E, Sedova L, Chylikova B, Kabelova A, Liska F, Seda O. Maternal high-sucrose diet affects phenotype outcome in adult male offspring: role of Zbtb16. Front Genet 2020;11:529421.
[52] Wetmore DR, Joseloff E, Pilewski J, Lee DP, Lawton KA, Mitchell MW, et al. Metabolomic profiling reveals biochemical pathways and biomarkers associated with pathogenesis in cystic fibrosis cells. J Biol Chem 2010;285(40):30516–22.
[53] Bass R, Brownell JN, Stallings VA. The impact of highly effective CFTR modulators on growth and nutrition status. Nutrients 2021;13(9).
[54] Wei Q, Pinho S, Dong S, Pierce H, Li H, Nakahara F, et al. MAEA is an E3 ubiquitin ligase promoting autophagy and maintenance of haematopoietic stem cells. Nat Commun 2021;12(1):2522.
[55] Lee MS, Han HJ, Han SY, Kim IY, Chae S, Lee CS, et al. Loss of the E3 ubiquitin ligase MKRN1 represses diet-induced metabolic syndrome through AMPK activation. Nat Commun 2018;9(1):3404.
[56] Cousin B, Cinti S, Morroni M, Raimbault S, Ricquier D, Penicaud L, et al. Occurrence of brown adipocytes in rat white adipose tissue: molecular and morphological characterization. J Cell Sci 1992;103(Pt 4):931–42.
[57] Wu J, Bostrom P, Sparks LM, Ye L, Choi JH, Giang AH, et al. Beige adipocytes are a distinct type of thermogenic fat cell in mouse and human. Cell 2012;150(2):366–76.
[58] Fisher FM, Kleiner S, Douris N, Fox EC, Mepani RJ, Verdeguer F, et al. FGF21 regulates PGC-1alpha and browning of white adipose tissues in adaptive thermogenesis. Genes Dev 2012;26(3):271–81.
[59] De Fano M, Bartolini D, Tortoioli C, Vermigli C, Malara M, Galli F, et al. Adipose tissue plasticity in response to pathophysiological cues: a connecting link between obesity and its associated comorbidities. Int J Mol Sci 2022;23(10).
[60] Loncar D. Convertible adipose tissue in mice. Cell Tissue Res 1991;266(1):149–61.

